Relative and absolute timing of tectonothermal events in the Pohjanmaa Belt: A structural study of the Paleoproterozoic coupled Bothnian oroclines, Finland

by

Travis Dawson
B.Sc., University of Vermont, 2014

A Thesis Submitted in Partial Fulfillment
Of the Requirements for the Degree of

MASTER OF SCIENCE

in the School of Earth and Ocean Sciences
UNIVERSITY OF VICTORIA

Supervisory Committee

Relative and absolute timing of tectonothermal events in the Pohjanmaa Belt: A structural study of the Paleoproterozoic coupled Bothnian oroclines, Finland

by

Travis Dawson
B. Sc., University of Vermont 2014

Supervisory Committee

Dr. Stephen T. Johnston (School of Earth and Ocean Sciences)
Co-Supervisor

Dr. Dante Canil (School of Earth and Ocean Sciences)
Co-supervisor

Dr. Kristin Morell (School of Earth and Ocean Sciences)
Departmental Member

Abstract

Supervisory Committee
Dr. Stephen T. Johnston (School of Earth and Ocean Sciences)
Co-Supervisor
Dr. Dante Canil (School of Earth and Ocean Sciences)
Co-supervisor
Dr. Kristin Morell (School of Earth and Ocean Sciences)
Departmental Member

Studies on the formation of oroclines (bends of originally linear mountain belts) are restricted to Phanerozoic examples. Here I provide a structural, metamorphic and geochronological study of the meta-sedimentary Pohjanmaa Belt, which lies on the most northerly limb of one of the few examples of Paleoproterozoic oroclines, the coupled Bothnian oroclines in Finland. My primary goal is to determine if the structures in the Pohjanmaa belt are consistent with the Svecofennian orogenic belt originating as a linear feature that was subsequently deformed into a pair of coupled oroclines.

My detailed structural mapping focused on the geometry of F_1, F_2, and F_3 folds within the Pohjanmaa Belt in west-central Ostrobothnia, Finland. Over 170 measurements were collected including interlimb angles, the attitudes of S_1 and S_2 foliations, and F_2 fold axes. Also, 28 oriented core samples were collected to conduct a U-Pb geochronological study of monazites and an analysis of metamorphic textures in thin section. I first provide a review and comparison of similar structures around the coupled Bothnian oroclines. In my structural analysis I address the relative timing of deformation and metamorphism and use new U-Pb monazite geochronological data to constrain the absolute timing of tectonothermal events. My findings suggest that: 1) D_1, D_2, D_3 deformation stem from a protracted event that records progressive deformation and strain partitioning from pure shear (D_1 shortening) to simple shear (D_2, D_3 sinistral shear) as a result of counter clockwise rotation; 2) D_2 folding and coeval garnet + staurolite metamorphism are consistent with early Svecofennian deformation, which occurred 80-90 m. y. prior to late-stage isothermal decompression and staurolite breakdown dated at 1.80 Ga by U-Pb monazite analysis; 3) My analysis, in combination with subsidiary data, provides evidence that sinistral shear during $D_{2\text{-}3}$ is the result of counter clockwise rotation of the Pohjanmaa belt possibly in response to buckling of the coupled Bothnian oroclines during the early Svecofennian Fennia event.

Table of Contents

List of Tables

List of Figures

Acknowledgments

I would first like to thank my supervisor Stephen T. Johnston for his guidance and tireless feedback no matter the geographic or time restrictions. His contributions Earth sciences are profound and inspired me to pursue this degree. He continually motivated me to persevere and reminded me of the importance of my research in the academic world. Thank you to Sayab Muhammad, for welcoming me to the Geological Survey of Finland, supporting me in the field, and for showing me all the possibilities within this project. Acknowledgments to the geoscientists at the GTK, whose involvement greatly improved my research. This includes Raimo Lahtinen, Tuomo Turunen, Bo Johanson, and Hugh O'Brien.

I would like to thank my committee members and other faculty at the University of Victoria with whom it has been my pleasure to work with and learn from during my studies. I am especially grateful for my fellow graduate students and friends at the School of Earth and Ocean Sciences, who provided me with endless support and created an enthusiastic atmosphere that grad school cannot be without.

I would not be capable of aspiring to achieve if not for my family. Thank you to my parents, Glenn and Shirley Dawson for providing every opportunity, and my siblings Aurora and Taylor Dawson whom I idolize. I am grateful for my partner and my friends who have provided me with endless happiness in all of life's journeys.

Funding for my Masters project was provided by an NSERC Discovery Grant that was awarded to my supervisor Stephen T. Johnston, and a University of Victoria Graduate award. Addition financial support was provided by the Geological Survey of Finland (GTK) for the field campaign and lab analysis portion of this research.

Chapter 1. Introduction

1.1 Motivation

The primary motivation for this thesis is to identify and further understand oroclines (bends of originally linear mountain belts). The term 'orocline' was first defined by Carey (1955) as an orogenic belt that has been curved about a vertical axis of rotation. Orocline formation is explained using two end-member processes that yield (Johnston et al., 2013) progressive and secondary oroclines respectively (Figure 1-1). Progressive oroclines are thin-skinned, meaning that they form in the crust above a basal decollement, and are suggested to be restricted to fold and thrust belts (Johnston et al., 2013). Bending of a progressive orocline is in response to ongoing crustal shortening, attributable to the original, orogen-perpendicular, principal compressive stress. Secondary oroclines are thick-skinned, form after initial thrusting and orogenesis has occurred, may involve deep crust and mantle, and are attributed to a near orthogonal switch in the principal compressive stress from orogen-perpendicular to orogen-parallel (Johnston et al., 2013).

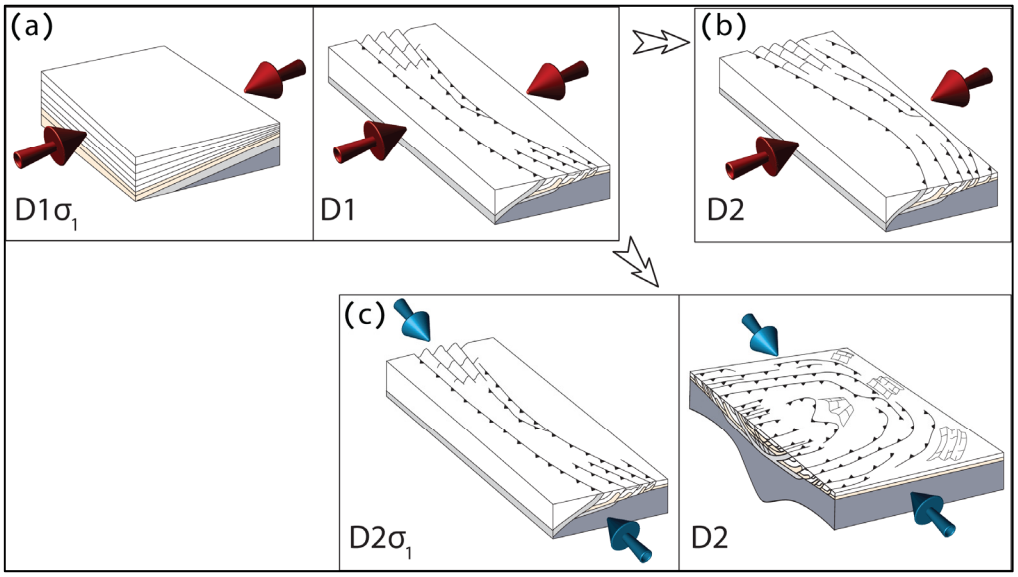

Figure 1-1 Diagram showing a) progressive and b) secondary models of orocline formation. (Johnston et al., 2013).

Previous studies provide examples of oroclines in Phanerozoic orogens (Johnston, 2001; Aerden, 2004; Van der Voo, 2004; Shaw et al., 2012; Shaw and Johnston, 2012; Johnston et al., 2013) and suggest that map-view curvature of orogens can be explained by syn- to post-orogenic buckling about vertical axes of rotation. Oroclines in Precambrian orogens are however, poorly documented, and the question of how they might differ from younger oroclines remains. This is due to a lack of well-exposed Precambrian terranes, and prolonged exposure to crustal recycling and erosion of the upper crust. Furthermore, paleomagnetic analysis, a standard test of oroclines, is commonly unavailable due to re-magnetization of Precambrian terranes during subsequent tectonothermal events. Therefore, when studying Precambrian oroclines, detailed structural analysis and mapping is required. Here I aim to provide a comprehensive structural and geochronological study of a hypothesized pair of Paleoproterozoic oroclines, the coupled Bothnian oroclines in Finland.

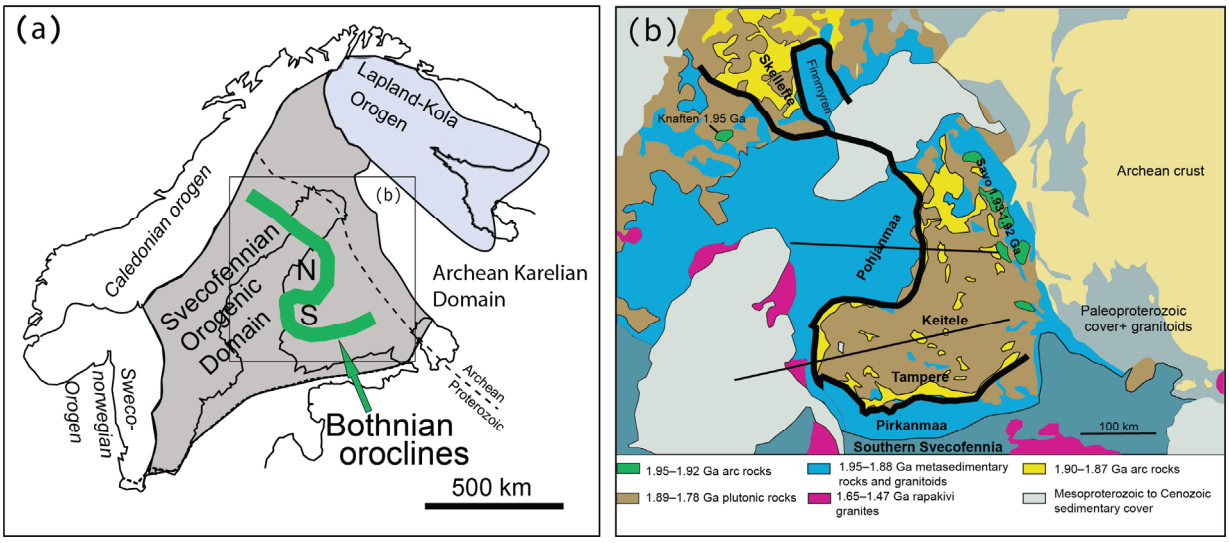

Figure 1-2 a) The major geological domains of the Fennoscandian Shield and the coupled Bothnian oroclines. b) The hypothesized trace of the coupled Bothnian oroclines as shown by sinuous crustal conductance anomaly (solid curved black line) and geological belts of the Svecofennian Orogenic Domain. Modified after Lahtinen et al. (2014).

Studying sinuous Precambrian orogens from the perspective of orocline processes can provide new insight into Precambrian plate tectonics. As an example, Lahtinen et al. (2014) have re-interpreted a well-studied portion of the Fennoscandian Shield in Finland as recording oroclinal buckling. They suggest that the Paleoproterozoic coupled Bothnian oroclines are comprised of two linked arcuate segments of the Svecofennian orogen, a northern convex-to-the east bend and a southern convex-to-the west bend that characterizes the Svecofennian Orogenic Domain (Figure 1-2). Lahtinen et al. (2014) provide a palinspastic restoration of the oroclines suggesting that the orogen originated as a 1000 km long, NW striking, linear orogen that was formed during arc-continent collision, and which was subsequently buckled into its present arcuate geometry (Figure 1-3). The Lahtinen et al. (2014) model proposes that the coupled Bothnian oroclines are secondary and formed as a result of an orthogonal switch in the orientation of principal compressive stress, initiating buckling of the Svecofennian orogen at 1.87 Ga. This thesis aims to test the aforementioned model through detailed analysis of the structures and metamorphism along the north limb of the northern of the two coupled Bothnian oroclines. My hypothesis states that structures around the oroclines are consistent with the linear Svecofennian orogen being subsequently deformed into its current arcuate geometry. Establishing the timing of, and the structures that characterize, the tectonothermal events throughout this segment of the Svecofennian orogen are important steps in validating the model for the formation of the Paleoproterozoic Bothnian oroclines in Finland.

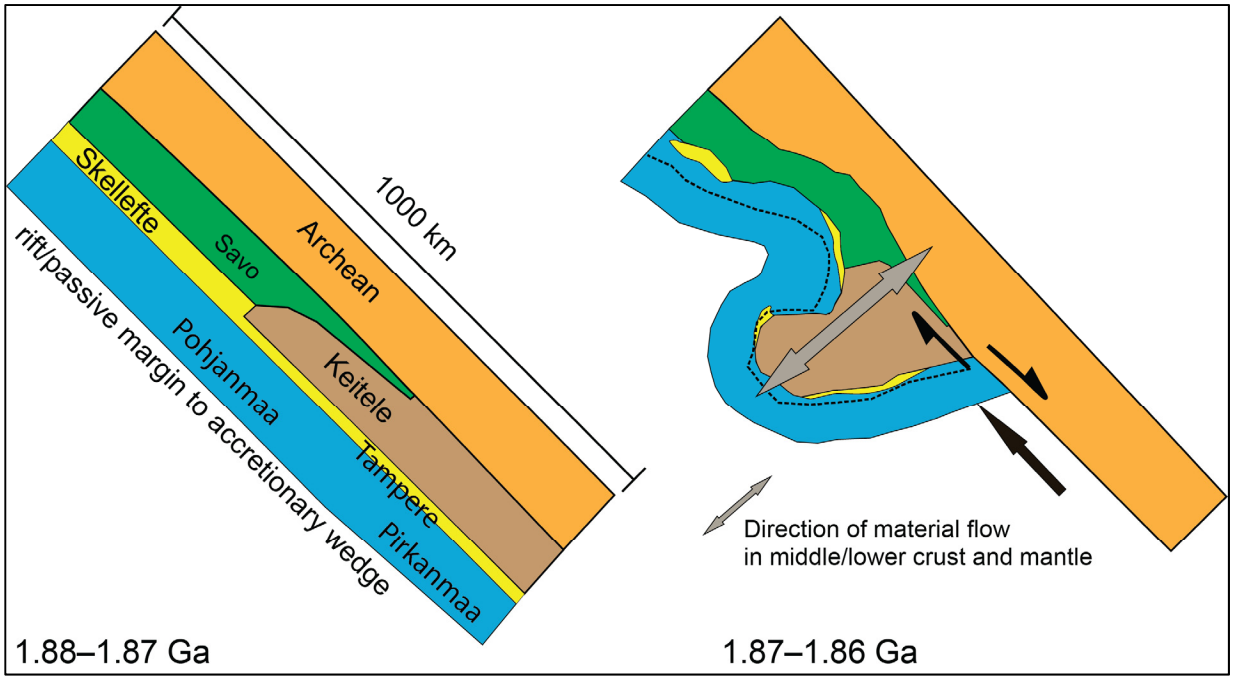

Figure 1-3 Model for the formation of the coupled Bothnian oroclines and buckling of the linear Svecofennian Orogen. Modified after Lahtinen et al. (2014).

1.2 Location of the study area

The study area is located in Central Ostrobothnia, which is a cooperative municipal region along the coast of the Gulf of Bothnia. My field area spanned approximately 100 x 100m and was located 5 km NE of the municipality of Himanka. There is little to no topographic relief as most of the area has been subjected to extensive glacial scouring and is < 50 m elevation above sea level. I conducted my study on a portion of the Pohjanmaa Belt that lies on the north most limb of the northern Bothnian orocline. In map view, the Pohjanmaa Belt is bent around the northern Bothnian orocline (Lahtinen et al., 2014) and is interpreted as one of a series of meta-sedimentary belts that make up a continuous and arcuate forearc complex in the Svecofennian Orogenic Domain (Figure 1-2).

1.3 Methods of Investigation

Fieldwork for this study was carried out from August 3rd to 12th, 2015. My field accommodation was located near the town of Lohtaja, while the town of Himanka was the main base for field operations. Besides initial guidance and setup from Dr. Sayab Muhammad, all fieldwork and mapping was carried out by the author with support from Tuomo Turunen, (Senior Field Assistant, GTK) who also operated the hand drill for core samples.

Fieldwork methods included mapping and measuring the geometry of folds along a series of transects (transects AB, CD, EF, GH), from 6-20m in length, on the flat glacially polished bedrock (Figure 1-4a). This method allowed for me to sketch the folds in detail and accurately record the location of structural measurements and core samples (Appendix: Figure A-1, Figure A-2, Figure A-3, Figure A-4, Figure A-5, Figure A-6). All structural measurements were taken with a CST Berger compass. My data consisted of interlimb angles and the attitudes of S_1 and S_2 foliations as well as F_2 fold axes. In some cases supporting data were acquired from oriented photographs (S_2, S_3, and interlimb angles). All structural analyses were completed using Stereonet® (Cardozo and Allmendinger, 2013). In total, 28-core sample locations were decided upon by the author and extracted by Tuomo Turunen using a hand held power drill (Figure 1-4b) with a 2.5 cm diameter diamond drill bit. All samples were oriented for north and any vertical discrepancy greater than 11˚ was corrected for using a Pomeroy orientation device. From the cores, 25 horizontal and 8 vertical thin sections were prepared and cut for SEM and LA-ICP-MS analysis.

Figure 1-4 Methods of investigation. a) Cleaning and exposing transects, featuring Sayab Muhammad; b) Operating the hand held drill, featuring Tuomo Turinen; c) Locating monazites on the SEM using EDS methods at the GTK headquarters; d) Operating the LA-ICP-MS system at the GTK headquarters; e) The laser ablation machine by Photon-Machine at the GTK headquarters; f) The ATTOM mass spectrometer machine by Nu-Instruments at the GTK headquarters.

Lab analysis took place from August 13th to August 28th, 2015, using the lab facilities at the Geological Survey of Finland (GTK) headquarters located in Espoo, a neighbouring municipality of Helsinki in southern Finland. After cutting and polishing thin-sections they were prepared for SEM scanning (Figure 1-4c), which was assisted by Senior GTK Lab Scientist Bo Johanson. Using energy dispersive spectrometry (EDS) analysis monazite grains were located within a coordinate system that was defined for each sample thin section. U-Pb isotope dating of the monazites was subsequently carried out using the LA-ICP-MS techniques. A laser-ablation system manufactured by Photon-Machine and a high-resolution Attom mass-spectrometer manufactured by Nu Instruments (Figure 1-4e, f) were used in the analysis. The LA-ICP-MS software recognizes the coordinates of each monazite grain and positions the machine in the precise location to ablate each grain individually. The ablated material is then carried to the mass spectrometry unit in a helium gas for isotope analysis. The isotope data is analyzed using Glitter software, and the age data was plotted using ISOPLOT concordia diagram software. All work on the LA-ICP-MS machine (Figure 1-4d), isotope analysis, and geochronological results was completed under the supervision of Senior GTK Isotopes Scientist Hugh O'Brien.

1.4 Previous Work

1.4.1 The Svecofennian Orogenic Domain in the Fennoscandian Shield.

The Fennoscandian (Baltic) Shield as defined by Gaal and Gorbatschev (1987) encompasses present-day Scandinavia and is comprised of late Archean to early Paleozoic continental crust. In Finland, the constituents that make up the Fennoscandian Shield (Figure 1-2) are the Archean Karelian Domain, the Lapland-Kola Orogen and the

Paleoproterozoic Svecofennian Orogenic Domain. The evolution of the Fennoscandian Shield began in the Paleoproterozoic with rifting and division of Archean crust into cratons, separated by newly developed ocean basins, from 2.5-2.0 Ga (Mouri et al., 1999; Lahtinen et al., 2008). Many studies (Nironen, 1997; Korja et al., 2006; Lahtinen et al., 2009b) have focused primarily on the subsequent amalgamation of rifted Archean cratons and Paleoproterozoic magmatic arcs to form the Svecofennian Orogenic Domain from 1.94- 1.79 Ga.

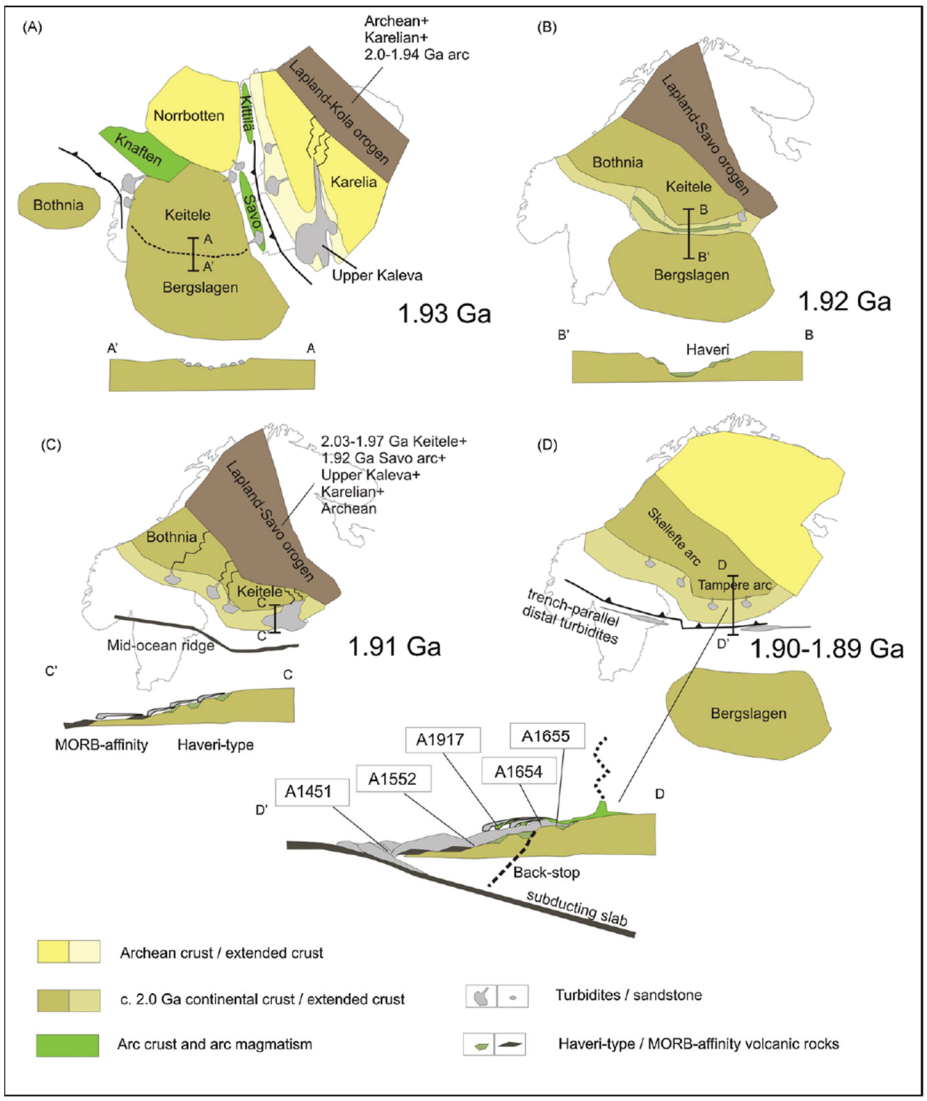

Figure 1-5 Tectonic model of arc accretion and sedimentation during the early Svecofennian orogenic phase. Modified after Lahtinen et al. (2009a).

In a tectonic synthesis published by Lahtinen et al. (2009b) it is suggested that growth of the Fennoscandian Shield is the result of multiple arc-continent collisional events from 1.92-1.79 Ga (Figure 1-5). This model explains the Svecofennian Orogenic Domain as the product of the closure of ocean basins, contemporaneous arc magmatism, and the accretion of exotic crustal segments to the Karelian Domain. Lahtinen et al. (2009b) divides the Svecofennian Orogenic Domain into four separate sub-orogens including: the Lapland-Savo, the Fennia, the Svecobaltic, and the Nordic. The Lapland-Savo (Figure 1-5a) and Fennia (Figure 1-5d) sub-orogens are interpreted to record arc-continent collisional processes during the early Svecofennian orogenic phase from 1.92-1.86 Ga (Ehlers et al., 1993; Skytta et al., 2006). The Svecobaltic and Nordic sub-orogens in the southeast and northwest portions of the Svecofennian Orogenic Domain, respectively, are interpreted to record continental collisions during a late Svecofennian orogenic phase from 1.835-1.79 Ga (Ehlers et al., 1993; Claesson and Lundqvist, 1995; Skytta et al., 2006).

Metamorphism throughout the Svecofennian Orogenic Domain is dominantly high-temperature/ low-pressure Buchan-type (Korsman et al., 1999). Thermodynamic modeling studies suggest that PT conditions range from 4-5 kbar and 650-700˚C and, in some cases, exceed 6 kbar and 800˚C (Vaisanen and Hölttä, 1999; Lind, 2013, unpublished data). A detailed metamorphic map of Finland (Hölttä and Heilimo, 2017) shows the regional distribution of low to high amphibolite grade and isolated granulite grade metamorphic assemblages. Two distinct metamorphic events, differentiated by timing and location, are outlined by Korsman et al. (1999). The first is an amphibolite grade event from 1.89-1.88 Ga, which is well documented in the western and central Svecofennian Orogenic Domain (Kilpelainen, 1998; Mouri et al., 1999; Rutland et al., 2004; Williams et al., 2008). Models

suggest prograde assemblages of aluminous phases are coeval with syn-orogenic magmatism, migmatization, and the development of D_2 structures during an early Svecofennian event. The second is a high-grade amphibolite to granulite event initiated at 1.835 Ga, which transitions to a high temperature/low pressure retrograde event until 1.79 Ga, primarily in the southern Svecofennian Orogenic Domain (Vaisanen and Hölttä, 1999; Vaisanen et al., 2002; Mouri et al., 2005; Skytta and Manttari, 2008; Torvela et al., 2008). Tectonic models suggest decompression and high geothermal gradients in areas that underwent crustal thinning and gravitational collapse (Nironen, 1997; Korja et al., 2006).

1.4.2 The Pohjanmaa Belt

The Pohjanmaa Belt in the vicinity of Himanka was first described by Salli (1964) as a package of supracrustal rocks consisting of pillow basalt, mica-quartz-feldspar schist to schistose greywacke with locally abundant metamorphic porphyroblasts. Salli (1964) suggested that the rocks have experienced as many as two near isoclinal folding events that exhibit orthogonal fold axes. Williams et al. (2008), based on a structural and geochronological study of the Evijärvi and Lappfors sub-groups of the Pohjanmaa belt surrounding Himanka, suggests that the Lappfors group lies unconformably below and records pre-1.91 Ga deformation and metamorphism not seen in the Evijärvi group. Williams et al. (2008) interpret the dominant ESE-WNW to NW-SE trending folds in the Evijärvi meta-sediments as products of a D_2 event, the timing of which is constrained by the 1.88 Ga age of peak metamorphism. Pre-1.91 Ga populations of detrital and metamorphic zircons in Svecofennian meta-sedimentary rocks were investigated by Lahtinen et al. (2009a). Their model suggests that Neoarchean and Paleoproterozoic zircon grains and their

metamorphic overgrowths are the result of sediment recycling from multi-phase orogenic events (Figure 1-5). Lahtinen et al. (2009a) propose coeval deposition of Svecofennian forearc basin sediments and magmatic arc volcanics.

1.5 Structure of Dissertation

Chapter 2, "Relative and absolute timing of tectonothermal events in the Pohjanmaa Belt: A structural study of the Paleoproterozoic coupled Bothnian oroclines, Finland", presents the results of a detailed analysis of deformation and metamorphism in the Pohjanmaa Belt, coupled with a U-Pb monazite geochronological study. I discuss the relative timing of D_1, D_2, and D_3 deformation and metamorphism, and place an absolute age constraint on a post-D_2 tectonothermal event. I then discuss the implications of my findings within the tectonic framework of the Svecofennian Orogenic Domain and propose a model for the formation of the coupled Bothnian oroclines. Chapter 2 was co-authored by Dr. Stephen T. Johnston and Dr. Sayab Muhammad, both of whom helped define the project and provided counsel throughout the writing process. Johnston supervised and helped the author highlight the importance of the project with regards to oroclinal processes. Muhammad assisted with fieldwork and data collection, and helped with the geochronological analysis. As first author, I led fieldwork and data collection, prepared samples, conducted SEM scans, preformed LA-ICP-MS analysis, undertook the analysis of fold geometries and metamorphic textures, and wrote the paper.

Chapter 3, "Conclusion" provides a summary of the findings of this thesis. My recommendations for future work suggests potential research ideas that may provide further insight to formation of the Paleoproterozoic coupled Bothnian oroclines.

Chapter 2. Relative and absolute timing of tectonothermal events in the Pohjanmaa Belt: A structural study of the Paleoproterozoic coupled Bothnian oroclines, Finland.

2.1 Introduction

Curvature, in map-view, is a common characteristic of orogenic belts, and Precambrian orogens are no exception. Precambrian orogens are events that stich together cratonic provinces and form geometrically equant portions of continental crust. The generation of continental crust is widely attributed to magmatic arcs. This, however, is problematic because magmatic arcs form long, linear tectonic features and how they become molded into equant continents is unclear. One explanation is that linear arc systems experience syn- to post-magmatic oroclinal buckling about a vertical axis of rotation (Johnston et al., 2013). The process of orocline formation, although still a topic of debate, provides a mechanism for developing equant portions of continental crust. Previous studies (Johnston, 2001; Aerden, 2004; Van der Voo, 2004; Shaw et al., 2012; Shaw and Johnston, 2012; Johnston et al., 2013; Weil et al., 2013; Del Greco et al., 2016) have documented Paleozoic and younger orogenic belts characterized by oroclines. Given the assumption that oroclines are products of plate tectonic processes and that plate tectonics was active in the Precambrian, then Precambrian orogens should also be characterized by oroclines (Van der Voo, 2004).

There remains, however, few well-documented Precambrian oroclines, for which there are several reasons. Foremost is the paucity of well-exposed Precambrian terranes as a result of younger rock cover overlying cratonic basement and the recycling of older crust. Secondly, the available exposures commonly comprise the mid- to deep-crust, meaning that tectonic vectors recorded in upper crust (i.e.; thrust sheets, carbonate-shale facies

transitions, shallow level intrusives and volcanics) of an orogen have been eroded away. Furthermore, testing models of Precambrian oroclines is difficult. Paleomagnetic techniques used as a tool for understanding oroclines (Eldredge et al., 1985; Van der Voo, 2004) are commonly unavailable because of secondary re-magnetization during younger tectonothermal events. Therefore, testing models of Precambrian oroclinal buckling relies on detailed mapping and structural analysis.

At least two potential Precambrian oroclines have been identified in the Archean - Paleoproterozoic Fennoscandian Shield of Scandinavia, including the Bergslagen orocline of Sweden (Beunk and Kuipers, 2012), and the coupled Bothnian oroclines of Finland (Lahtinen et al., 2014). To test the coupled Bothnian orocline model, I studied the structural evolution of the Pohjanmaa belt, a geological unit of the Paleoproterozoic Svecofennian Orogenic Domain (Figure 2-1 and Figure 2-2) that lies along the hypothesized north limb of the northern of the two coupled Bothnian oroclines. Also, I undertook a detailed geochronological analysis of monazites, allowing me to constrain the timing of deformation and metamorphism. Here a review of previously established constraints is provided on the nature and timing of Svecofennian deformation and metamorphism. I then present my new structural and metamorphic data, and provide a structural analysis, including addressing the relative timing of deformation and metamorphism. New U-Pb monazite geochronological data is then used to constrain the absolute and relative timing of tectonothermal events. The main question addressed is did the Svecofennian orogenic belt originate as a linear feature that was subsequently deformed into a pair of coupled oroclines. Finally, I discuss whether the structures and metamorphism are consistent with coupled Bothnian orocline model and what the implications of my findings are.

2.2 Geological Setting

2.2.1 Regional Geology

A large portion of the Fennoscandian Shield is comprised of the Paleoproterozoic Svecofennian Orogenic Domain (Figure 2-1 and Figure 2-2) . The Svecofennian Orogenic Domain is thought to have formed between 1.92 to 1.79 Ga (Korja et al., 2006), with the bulk of the crustal growth occurring during two main orogenic phases: 1) the early Svecofennian from 1.92-1.86 Ga and 2) the late Svecofennian from 1.835-1.79 Ga. The time period in between the early and late Svecofennian orogenic phases, from 1.86-1.84 Ga, is interpreted as a period of shield-wide extension and gravitational collapse (Lahtinen, 1997; Korja et al., 2006). The early Svecofennian orogenic phase (Ehlers et al., 1993; Skytta et al., 2006) is described by Lahtinen et al. (2009b) as a combination of microcontinental and magmatic arc collision with the Archean Karelian Domain during the Lapland-Savo event from 1.92-1.91 Ga, and subsequent accretion of exotic crustal segments to the Fennoscandian continent during the Fennia event from 1.89-1.86 Ga (Figure 2-1 and Figure 2-3). The late Svecofennian orogenic phase (Ehlers et al., 1993; Claesson and Lundqvist, 1995; Skytta et al., 2006) is described by Lahtinen et al. (2009b) as a period of collision between the Fennoscandia and Sarmatia crustal blocks during the Svecobaltic event from 1.835-1.79 Ga, and between the Fennoscandian and Amazonian crustal blocks during what has been referred to as the Nordic event from 1.82-1.79 Ga (Figure 2-1). Evidence of crustal deformation attributed to the early Svecofennian ‘Fennia’ and late Svecofennian ‘Svecobaltic’ events is recorded in three critical geological regions (Figure 2-2): the Southern Svecofennian Arc Complex , the Central Svecofennian Arc Complex , and the Bothnian Arc Complex . The following provides on overview of these regions.

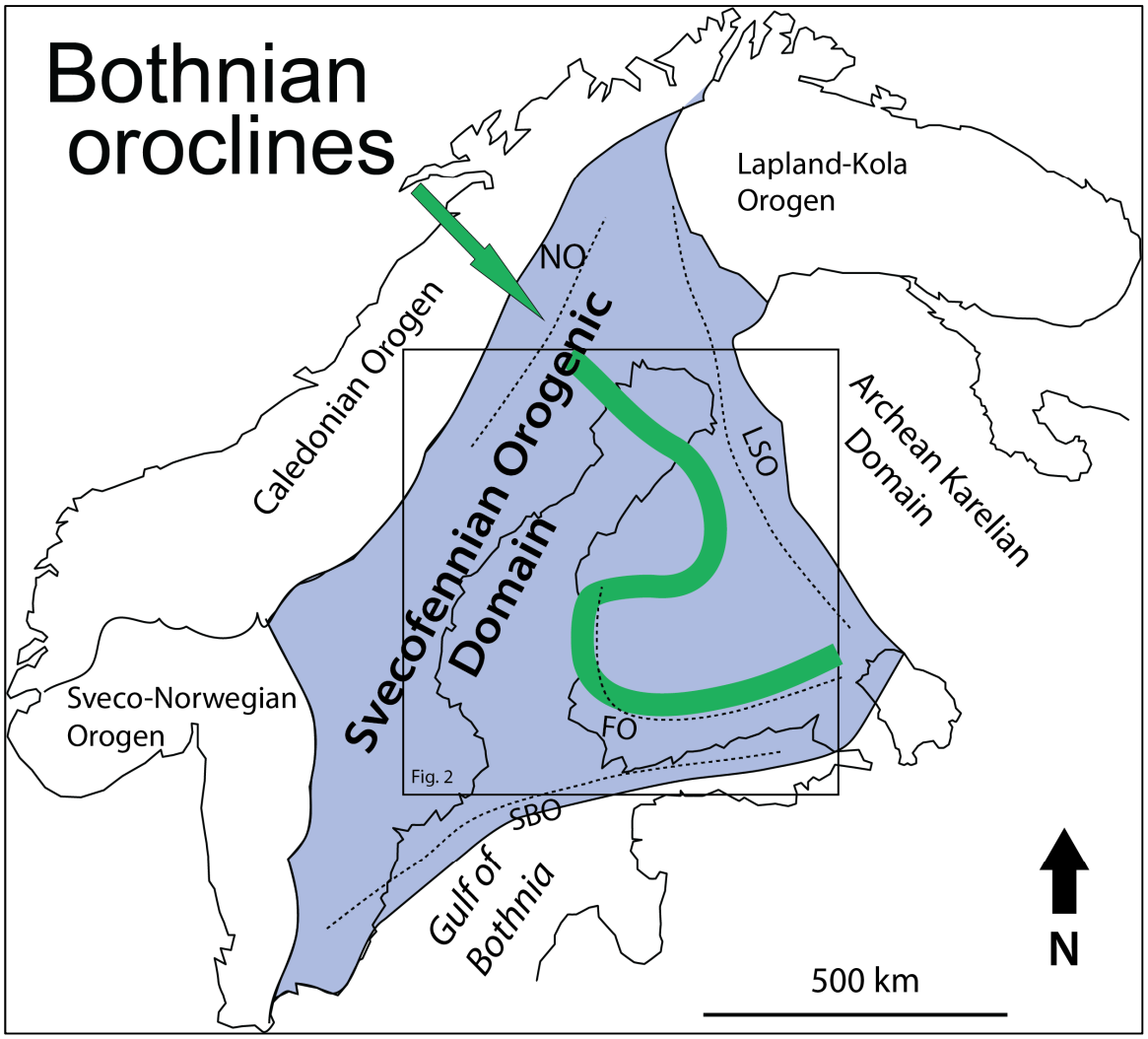

Figure 2-1 The major geological domains of the Fennoscandian Shield, The Paleoproterozoic Svecofennian Orogenic Domain (blue) is comprised of 4 major orogens; the LSO, Lapland-Savo orogen; FO, Fennia orogen; SBO, Svecobaltic orogen; NO, Nordic orogen. The location of the coupled Bothnian oroclines is indicated by the green line. Modified after Lahtinen et al. (2014)

The Southern Svecofennian Arc Complex (Figure 2-2) is immediately south of and is separated from the Central Svecofennian Arc Complex by what is inferred to be a suture zone. The Southern Svecofennian Arc Complex is characterized by three E-W trending geological belts. These belts are, from north to south, the Häme, Uusimaa and Turku, and together they constitute a collage of arc-type volcanic rocks, intermediate to felsic intrusive

rocks, rift related basalts and marine sediments (Vaisanen and Hölttä, 1999; Skytta et al., 2006). Rocks of the Southern Svecofennian Arc Complex have been metamorphosed to amphibolite to granulite grade and are complexly deformed (Vaisanen et al., 2002; Mouri et al., 2005; Skytta and Manttari, 2008). The Southern Svecofennian Arc Complex belts are interpreted as exotic crustal segments, which were first amalgamated and then were subsequently accreted to the Central Svecofennian Arc Complex.

The Central Svecofennian Arc Complex (Figure 2-2) in central Finland is characterized by two E-W trending geological belts, the northerly Tampere and the more southerly Pirkanmaa. These belts lie south of the Central Finland Granitoid Complex that makes up the core of the Svecofennian Orogenic Domain. The Tampere Belt is composed of arc type meta-volcanic rocks that overlie turbiditic meta-greywackes and MORB/WPB basalts. The Pirkanmaa Belt, also referred to as the Vammala Belt (Nironen, 1989; Kilpelainen, 1998), consists of migmatites and gneisses of sedimentary origin and syn-kinematic granitoids. Although separated by a sharp boundary, Lahtinen et al. (2009a) suggested that the Tampere and Pirkanmaa belts evolved contemporaneously and represent an early Svecofennian south-facing volcanic arc overriding a N to NE directed subduction zone (Figure 2-3) and a more ocean ward forearc accretionary wedge, respectively (Nironen, 1997; Lahtinen et al., 2009b; Chopin et al., 2014).

The Bothnian Arc Complex lies north of the Central Svecofennian Arc Complex (Figure 2-2) and encompasses primarily Paleoproterozoic supracrustal rocks. It is characterized by the Robertsfors Group and Skellefte District of eastern Sweden and the Pohjanmaa Belt of western Finland. The Skellefte District is characterized by felsic volcanic rocks and is bound to the south by the meta-sedimentary Robertsfors Group (Rutland et al., 2001a; 2001b). The

Robertsfors Group is interpreted to represent an accretionary wedge that lay in the forearc of a south-facing Skellefte district magmatic arc (Figure 2-3). Together, the Robertsfors Group and Skellefte District are interpreted as being a continuation of the Tampere-Pirkanmaa Belts of the Central Svecofennian Arc Complex (Lahtinen et al., 2014). The Pohjanmaa Belt consists of migmatitic, amphibolite grade mica schists and gneisses. Protoliths include turbiditic greywackes and mud-rocks (Lehtonen et al., 2005; Williams et al., 2008; Lahtinen et al., 2009a). Metamorphosed basalt, shale, chert, carbonate and granitoid intrusions are also present. The rock associations and metamorphism of the Pohjanmaa Belt are similar to the Robertsfors Group and the Pirkanmaa Belt. The Pohjanmaa Belt has a curved map profile and it is suggested that together, with the Robertsfors and the Pirkanmaa, these belts form a larger continuous albeit highly curved early Svecofennian meta-sedimentary belt (Figure 2-2)(Lahtinen et al., 2014). This sedimentary belt preserves a record of a closed back-arc basin and voluminous deposition of sediments eroding ocean-ward off of adjacent magmatic arc systems along a newly developed subduction zone. Such an interpretation implies that the combined Robertsfors - Pohjanmaa - Pirkanmaa Belt is part of a continent-scale forearc complex (Figure 2-3).

Lahtinen et al. (2014) argued that the continuity of the highly sinuous volcanic and forearc meta-sedimentary belts was best explained as a result of oroclinal buckling of a formerly linear, NW-SE striking early Svecofennian Fennia orogen (Figure 2-2). Evidence of buckling is shown by the change in the direction of prograde metamorphism and tectonic vectors as a function of strike around the coupled Bothnian oroclines. Their model involves oroclinal buckling shortly after arc-continent collision at around 1.87 Ga and requires a post-orogenic switch in compressive stress. Lahtinen et al. (2014) also attribute tightening of the

southern oroclinal limb and coeval thermal overprinting to NW-SE continental collision during the 1.83-1.80 Ga Svecobaltic orogen.

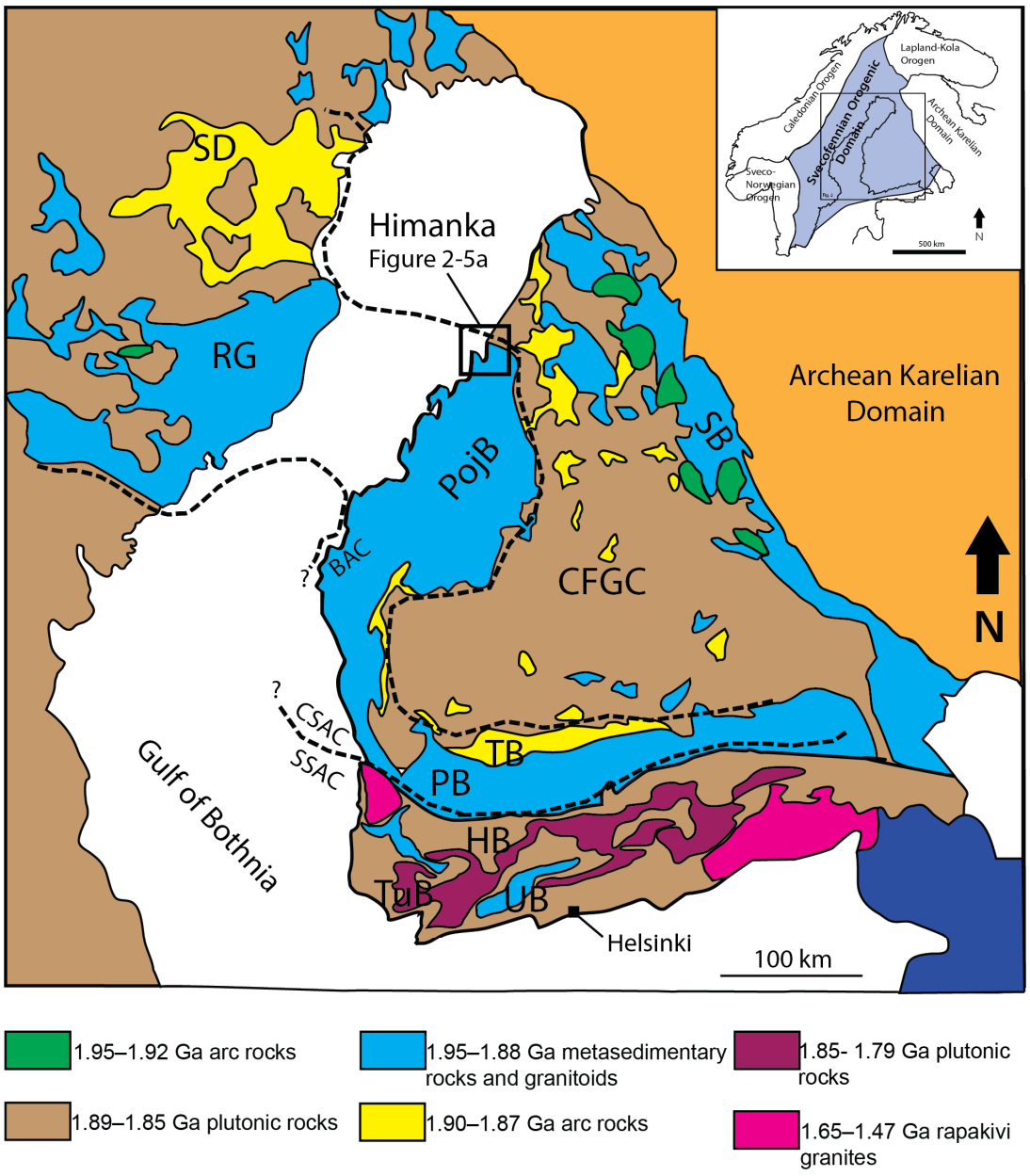

Figure 2-2 Geological regions and belts across the Paleoproterozoic Svecofennian Orogenic Domain (see Figure 1). The coupled Bothnian oroclines are indicated by dashed lines, which outline the arcuate Geological regions; BAC-Bothnian Arc Complex, CSAC-Central Svecofennian Arc Complex, SSAC-Southern Svecofennian Arc Complex. The geological belts that make up these regions are also shown; PojB-Pohjanmaa Belt, SD-Skellefte District, RG-Robertsfors Group, TB-Tampere Belt, PB-Pirkanmaa Belt, CFGC-Central Finland Granitoid Complex, SB-Savo Belt, HB-Häme Belt, UB-Uusimaa Belt, TuB-Turku Belt. Location of study area at Himanka. Modified after Lahtinen et al. (2009a) and Lahtinen et al. (2014).

2.2.2 Early Svecofennian Orogenic Phase / 'Fennia' Event

The following data are compiled from previous studies. D_1 and D_2 structures in the Southern Svecofennian Arc Complex, Central Svecofennian Arc Complex, and Bothnian Arc Complex are inferred to have developed during, and provide a record of the early Svecofennian Fennia event. Throughout the Svecofennian Orogenic Domain, D_1 fabrics commonly consist of layer-parallel schistose foliations $S_0//S_1$ (Nironen, 1989; Kilpelainen, 1998; Vaisanen and Hölttä, 1999; Rutland et al., 2001a; Williams et al., 2008). F_1 folds are tight to isoclinal and vary from upright to recumbent. F_1 fold hinges are rare and are commonly obliterated by subsequent deformation. The S_1 foliation is interpreted to have developed as a sub-horizontal cleavage that was axial planar to isoclinal recumbent F_1 folds formed during the early Svecofennian orogenic phase (Kilpelainen, 1998; Lahtinen et al., 2009b). D_1 metamorphism varied from greenschist to amphibolite facies. Syn-D_1 garnet-cordierite-andalusite-staurolite assemblages are common in meta-sedimentary rocks throughout the Bothnian Arc Complex and the Central Svecofennian Arc Complex (Kilpelainen, 1998; Rutland et al., 2004; Williams et al., 2008).

The timing of D_1 is poorly constrained. Volcaniclastic and pelitic sedimentary rocks were deposited in pre-orogenic basins between 1.95-1.92 Ga and during syn-orogenic crustal subsidence between 1.92 and 1.87 Ga (Lundqvist et al., 1998; Rutland et al., 2001b; Lahtinen et al., 2009a). Basalts (WPB and MORB), shales and the lowermost turbidites (1.92-1.91 Ga) of the Bothnian Arc Complex and the Central Svecofennian Arc Complex are syn-orogenic and were deposited during the collisional Lapland-Savo event (Figure 2-3). These rocks are overlain by an upper arc-derived turbidite sequence (≤1.90 Ga) that makes up the Robertsfors – Pohjanmaa – Pirkanmaa forearc complex (Lahtinen et al., 2002). Deposition

within the forearc complex was deposited coeval with subsidence and deformation during the Fennia event (Lahtinen et al., 2009a), and likely marks the initiation of D_1. Syn-kinematic D_2 intrusions crystallized as early as 1.896 Ga (Williams et al., 2008), but more commonly yield emplacement ages of 1.88-1.86 Ga in the Bothnian Arc Complex, Central Svecofennian Arc Complex and Southern Svecofennian Arc Complex (Nironen, 1989; Claesson and Lundqvist, 1995; Kilpelainen, 1998; Rutland et al., 2001b; Vaisanen et al., 2002) and provide a minimum age constraint for D_1. Hence, D_1 is constrained to the 10 m.y. period between 1.90 and 1.89 Ga (Kilpelainen, 1998) (Figure 2-4).

D_2 structures include shear zones and open to isoclinal, steeply plunging to recumbent folds in the Bothnian Arc Complex (Rutland et al., 2001a; 2001b; Williams et al., 2008), and open to isoclinal, typically upright folds in the Southern Svecofennian Arc Complex and Central Svecofennian Arc Complex (Nironen, 1989; Kilpelainen, 1998; Vaisanen and Hölttä, 1999; Skytta et al., 2006). F_2 folds are commonly refolded and their fold axes plunge moderately to steeply east and west. S_2 is an axial planar, often sub-vertical, micaceous axial planar schistosity (Nironen, 1989; Kilpelainen et al., 1994; Rutland et al., 2001a; Skytta et al., 2006). The development of S_2 involved the crenulation and local obliteration of the $S_o//S_1$ foliation, and F_2 folds result in steepening of the S_1 foliation. The strike of F_2 axial traces commonly sub-parallels the arcuate margins of geological belts (Lahtinen et al., 2017). Regional amphibolite grade metamorphism was coeval with D_2. Garnet-staurolite-andalusite and garnet-cordierite-sillimanite commonly grow along and define the S_2 axial planar foliation. D_2 shortening has been attributed to prolonged compression during NE to ENE directed subduction in the Bothnian Arc Complex (Nironen, 1997; Lahtinen et al., 2009a) and N to NNE directed subduction in the Central Svecofennian Arc Complex (Lahtinen et al.,

2009a) (current coordinates). Subduction in the Central Svecofennian Arc Complex is assumed to have led to island arc collision and the closure of the ocean that separated the Central Svecofennian Arc Complex and the Southern Svecofennian Arc Complex (Kilpelainen et al., 1994; Koistinen et al., 1996; Vaisanen et al., 2002; Skytta et al., 2006; Lahtinen et al., 2009b). Minor gravitational collapse following the early Svecofennian Fennia event (Korja and Heikkinen, 2005; Lahtinen et al., 2009b), and the resulting extension explains post-orogenic intrusions (Nironen et al., 2000) in the Central Finland Granitoid Complex (CFGC, Figure 2-2).

The D_2 tectonothermal event is well documented, and its timing well constrained throughout the Svecofennian Orogenic Domain. In the Bothnian Arc Complex, 1.896 Ga granitoids intrude the Finnish Pohjanmaa Belt and are deformed by a 1.88 Ga D_2 event, which is dated by metamorphic zircon and monazite (Williams et al., 2008). Syn-orogenic intrusions from the Swedish portion of the Bothnian Arc Complex provide younger ages for D_2 from 1.877-1.86 Ga (Claesson and Lundqvist, 1995; Rutland et al., 2001a; 2001b). In the Central Svecofennian Arc Complex metamorphism peaked at 1.880 Ga, the age of D_2 metamorphic monazite and zircon from migmatites (Mouri et al., 1999; Rutland et al., 2004), and was coeval with syn-orogenic intrusions that crystallized between 1.885 and 1.880 Ga (Nironen, 1989; Kilpelainen, 1998). In the Southern Svecofennian Arc Complex, D_2 is slightly younger than in the Central Svecofennian Arc Complex and is constrained by 1.88 to 1.86 Ga (Vaisanen et al., 2002; Skytta et al., 2006) syn-orogenic intrusions (Figure 2-4).

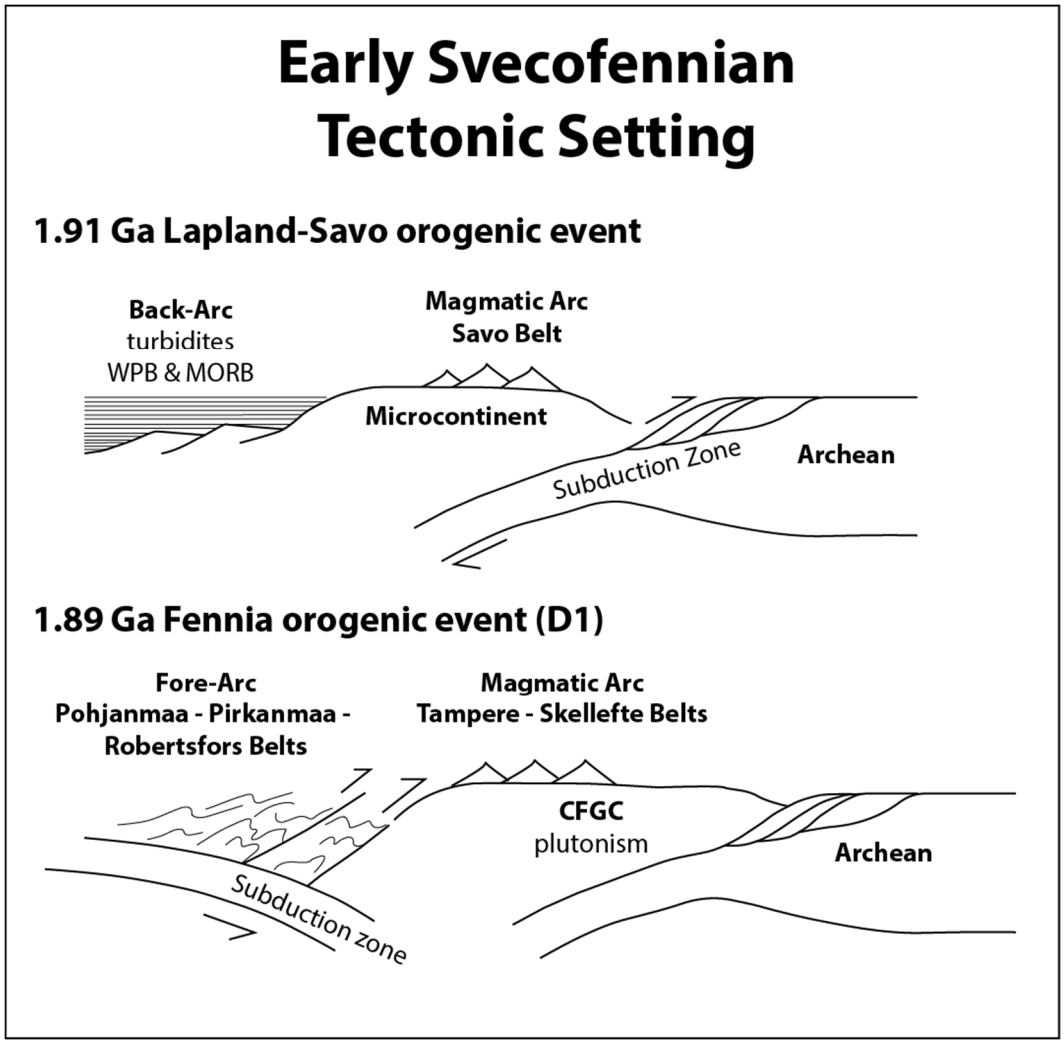

Figure 2-3 Cross-sectional views of the tectonic setting in the Bothnian Arc Complex and Central Svecofennian Arc Complex during the early Svecofennian orogenic phase. Modified after Chopin et al. (2014).

2.2.3 Late Svecofennian Orogenic Phase / 'Svecobaltic' Event

The following data are compiled from previous studies. D_3 and D_4 structures in the Bothnian Arc Complex, Central Svecofennian Arc Complex, and Southern Svecofennian Arc Complex are inferred to have developed during, and provide a record of, late Svecofennian orogenesis during the Svecobaltic event. Deformation associated with the Nordic event is only observed in northern Lapland and Sweden (Korja et al., 2006; Lahtinen et al., 2009b). The geometry of D_3 structures varies throughout the Svecofennian Orogenic Domain. In the

Central Svecofennian Arc Complex, F_3 kink folds have steeply dipping axial planes that strike NW-SE and NNE-SSW. The folds are asymmetric and show dextral and sinistral vergence (Nironen, 1989). In the Southern Svecofennian Arc Complex, F_3 folds are the dominant regional structures. Although F_3 varies in structural style, from upright to inclined to recumbent, the F_3 axial traces trend consistently E-W (Vaisanen and Hölttä, 1999; Vaisanen et al., 2002; Skytta et al., 2006; Skytta and Manttari, 2008). Intrusive dikes and pegmatite veins (1.835-1.825 Ga) are syn-kinematic with F_3 folding in the Uusimaa Belt (Skytta et al., 2006; Skytta and Manttari, 2008; Torvela et al., 2008). Garnet-cordierite-andalusite-sillimanite porphyroblasts post-date and overgrow S_1 and S_2 foliations and indicate peak metamorphism coeval with D_3 at 1.832-1.816 Ga (Mouri et al., 2005) and 1.824 Ga (Vaisanen et al., 2002). In the Bothnian Arc Complex, Claesson and Lundqvist, (1995) describe late-orogenic 1.822 Ga granite plutons that are geochemically similar to granites of the Southern Svecofennian Arc Complex granitoid-migmatite belts (Figure 2-4). D_4 is characterized by upright to inclined, E-W striking folds that deform D_3 foliations and are coeval with crustal melting and syn-kinematic granite/pegmatite intrusions from 1.82-1.81 Ga (Skytta and Manttari, 2008). D_4 brittle-ductile N-S and NW-SE striking shear zones are characterized by related folds, faults, and fracture sets (Vaisanen and Hölttä, 1999; Skytta et al., 2006).

D_3 and D_4 structures are characteristically distinct, however, they may be at least in part coeval. Lahtinen (unpublished data, 2017) suggests that 1.83 Ga D_4 structures are common across the Fennoscandian continent. Complex folding during D_3 and the subsequent development of D_4 folds and shear zones has been interpreted to reflect N-S shortening followed by a switch to more E-W directed transpression as a result of oblique continental collision during the Svecobaltic event (Vaisanen et al., 2002; Skytta et al., 2006). Following

collision, the crust underwent major re-stabilization in the form of gravitational collapse, which is attributed with high temperature/low pressure metamorphism of the lower crust of the Svecofennian Orogenic Domain and subsequent exhumation after 1.79 Ga (Korja et al., 2006; Torvela et al., 2008)(Figure 2-4). In summary, D_3 and D_4 fabrics and structures found throughout Fennoscandia formed between 1.835-1.81 Ga and partially overlapped with decompression and rapid cooling, which marked the end of Svecofennian orogenesis.

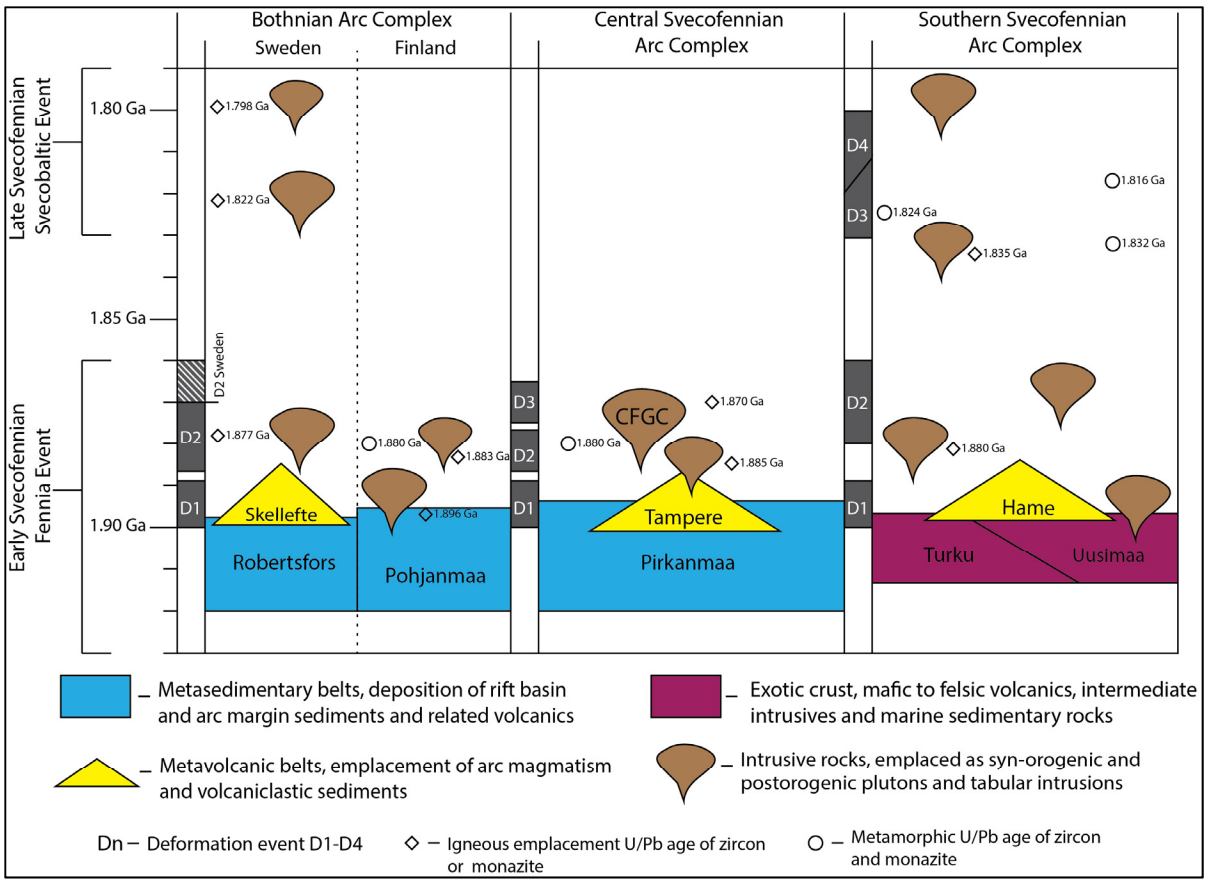

Figure 2-4 Geological time-line for the critical regions of the Svecofennian Orogenic Domain.

2.2.4 The Pohjanmaa Belt in Himanka

The study area is situated 5 km NE of the Himanka Township, in the Bothnian Arc Complex of western Finland (Figure 2-5). Rocks near Himanka have been included in the

Pohjanmaa belt and consist of mafic meta-volcanics and meta-sedimentary schists that range from quartz-feldspar to mica schist with locally abundant porphyroblasts (Salli, 1964). The sequence is divisible into the Evijärvi and the Lappfors groups. The Lappfors Group is thought to represent a basement complex (Williams et al., 2008). The Evijärvi Group consists of metamorphosed turbiditic greywackes and mud-rocks with a maximum depositional age of 1.92-1.91 Ga (Lahtinen et al., 2009a) that are inferred to be younger than and to unconformably overlie the Lappfors Group. In the area surrounding Himanka, the Niska granitoid (1.896 Ga) and the Rautio batholith (1.883 Ga) are interpreted as early Svecofennian plutons that intruded during and formed part of a thermal event that is also recorded by ~1.88 Ga zircon overgrowths in the Pohjanmaa meta-sediments (Williams et al., 2008).

The study area is underlain by amphibolite grade biotite schists of the Evijärvi Group that are exposed on sub-horizontal, flat, glacially scoured, surfaces (Figure 2-5c). Primary sedimentary bedding is locally recognizable and consists of turbiditic, fining-upward, interbedded psammitic and pelitic layers (Figure 2-6a). Bedding is folded; overprinting relationships indicate as many as three deformational events. The earliest foliation is a layer-parallel $S_o//S_1$ biotite schistosity. $S_o//S_1$ was folded; a pervasive S_2 biotite schistosity is axial planar to upright, steeply east plunging F_2 folds (Figure 2-7). F_3 kink-bands are characterized by vertical axial planes and deform the F_2 folds. Quartz veins and felsic and mafic dikes are folded by F_2 and are sub-parallel to the $S_o//S_1$ foliation (Figure 2-6b, c, d). The felsic dikes are granodioritic to tonalitic in composition and have 1-2 cm thick chilled margins. The presence of biotite, garnet, staurolite, cordierite and andalusite porphyroblasts (Figure 2-10) in metapelites is indicative of high temperatures and medium to low

pressures, during amphibolite grade metamorphism.

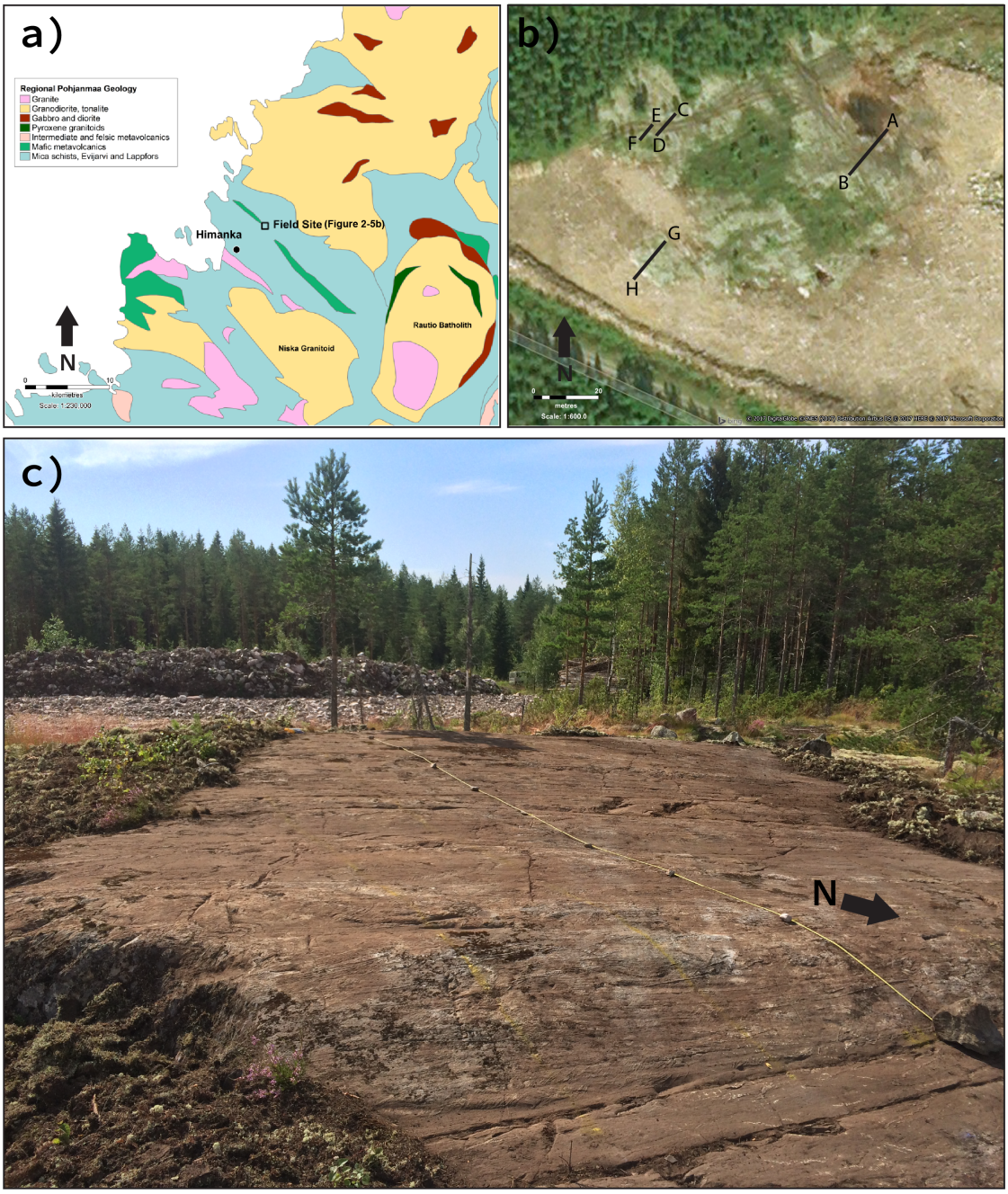

Figure 2-5 a) Regional geology of the Pohjanmaa belt and location of field site. b) Orthophoto of the Himanka field site and location of transects AB, CD, EF, GH. C) Transect CD at Himanka field area. The line trends along a 030° NE heading and the cobble markers on the tape measure are 1 meter apart.

2.3 Structural Analysis and Interpretations

2.3.1 Field Methods

Collection of structural data was accomplished by detailed mapping of flat, glacially polished exposures along a series of transects (AB, CD, EF, and GH) 6-20 meters long and 2-4 meters wide, trending 030˚ (Figure 2-5b, c). The location of structural measurements and core sample locations were recorded along each transect. The geometry of F_2 and F_3 folds (interlimb angles, dip angle of foliations and strike of axial planes) was constrained by field measurements and oriented photographs. All structural data measured from the field and oriented photographs was analyzed using Stereonet® software (Cardozo and Allmendinger, 2013). Fold sets and foliations, and their attributed deformation events are described sequentially below.

2.3.2 D_1 Structures

Bedding (S_o) is defined by turbiditic fining upwards sequences, which indicate that the sequence is upright and youngs to the East (Figure 2-6a). A NE-dipping, NW-striking (Figure 2-6 and Figure 2-7) foliation (S_1) defined by aligned biotite grains is sub-parallel to the primary bedding (S_o//S_1). Parallelism of S_o and S_1 imply that F_1 folds are isoclinal. Quartz veins and felsic to mafic dikes are also sub-parallel the S_0//S_1 foliation and are boudinaged (Figure 2-6b, c, d). Although difficult to measure, the long axes of boudins (L_1), which can be used as a proxy for F_1 axes, plunge steeply and are roughly parallel to the plunge of F_2 fold axes. The S_o//S_1 sub-parallel veins and dikes are interpreted as early magmatic and metamorphic products of D_1 that were flattened into parallelism with and extended and boudinaged along the S_1 axial plane during F_1 isoclinal folding (Figure 2-6). The style of D_1 deformation is consistent with early Svecofennian structures observed by Williams et al.

(2008) that are characterized by isoclinal fold hinges.

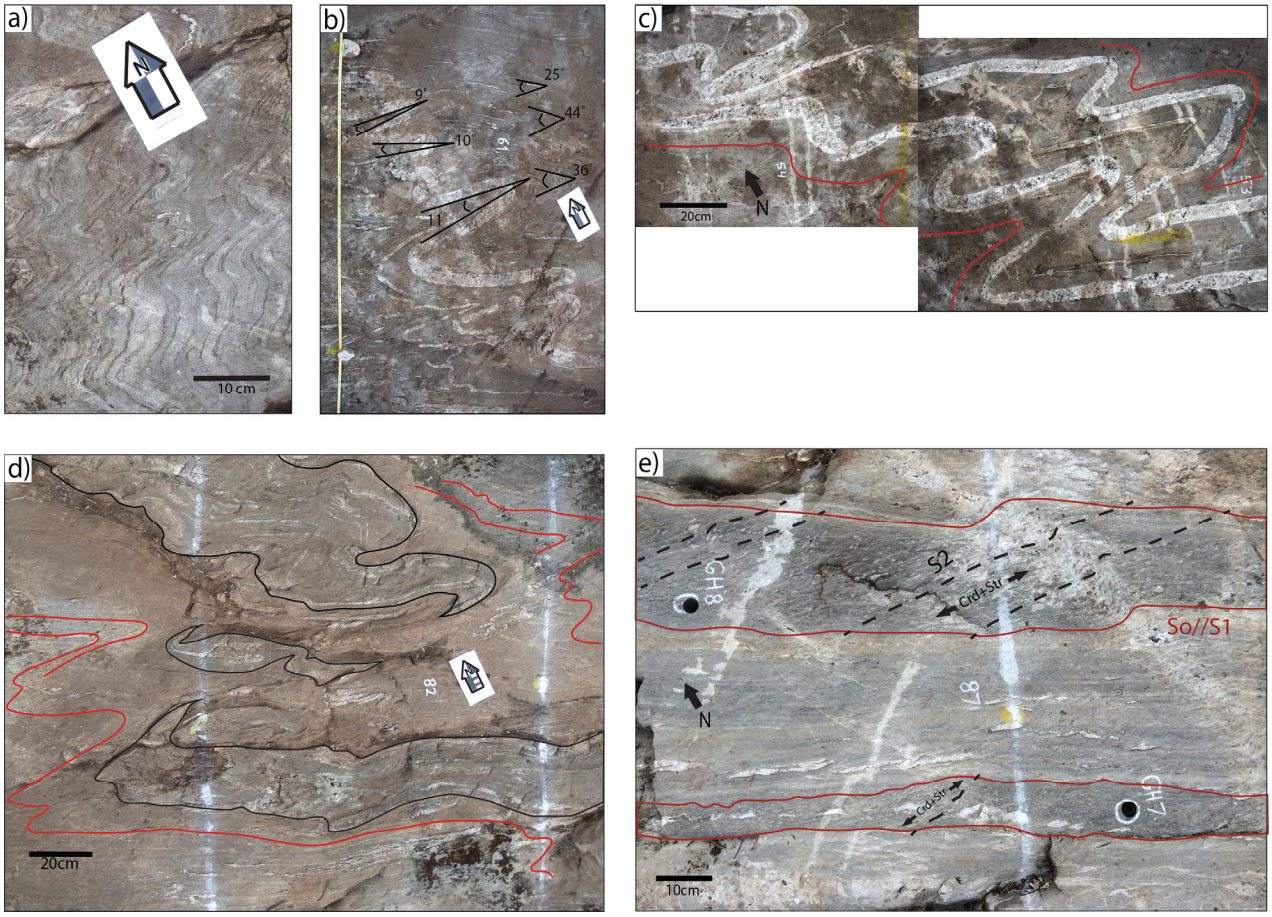

Figure 2-6 a) Turbiditic bedding sequences and S_o//S_1 foliation (transect EF). b) Interlimb angles of F_2 folds of a felsic dike, quartz veins and S_1 foliation in host rock (transect CD). c) F_2 folds of D_1 boudins of felsic (transect AB) and d) mafic dikes (transect GH). Dikes sub-parallel S_o//S_1 foliation (red lines). e) Pelitic beds (red lines) parallel to S_o//S_1. The S_o//S_1 and S_2 (dashed black lines) foliations are folded by F_3 kink folds (transect GH).

2.3.3 D_2 Structures

S_o//S_1 is folded. In the low strain hinge regions of F_2 folds, S_1 strikes ~N to NNE and dips steeply east (Figure 2-8a), which may reflect the original orientation of S_1 prior to F_2 folding (Sayab, 2009). An S_2 axial planar foliation is defined by the parallel alignment of biotite (S_2) and by aligned quartz and minor muscovite and chlorite. S_2 is sub-vertical and strikes WNW-ESE (Figure 2-7and Figure 2-8b). In thin section, the S_2 foliation in F_2 fold

hinge regions are defined by stage 3-4 crenulation cleavage development (Figure 2-10f) (terminology after Bell and Rubenach, 1983), whereas along F_2 fold limbs, S_2 is sub-parallel to $S_o//S_1$. F_2 folds plunge moderately to steeply towards ESE (Figure 2-7and Figure 2-8c) and exhibit asymmetrical, SE verging, Z-geometry fold trains. Where the F_2 folds affect quartz veins and dikes (Figure 2-6b), they are tight to isoclinal (Interlimb angle= 26˚-0˚, n=12), whereas F_2 folds of the meta-sedimentary host rock are close to tight (Interlimb angle=60˚-18˚, n=12). The Z-geometry fold trains consist of tightly folded hinge regions that step laterally and are connected through elongate, planar F_2 fold limb regions (Figure 2-7). Within the tightly folded hinge regions, D_1 boudins are deformed and stacked (Figure 2-6b, c, d). In F_2 fold limbs, layer parallel veins are thinned and stretched along the $S_o//S_1$ foliation.

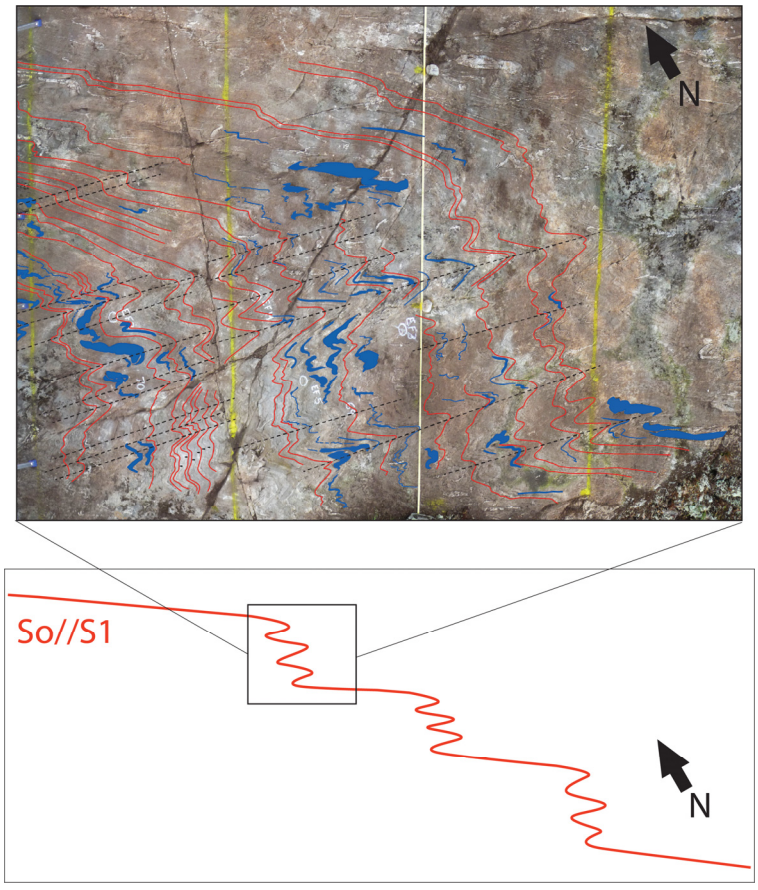

Figure 2-7 Photomosaic of transect EF showing F_2 folds (upper) and overall F_2 fold train geometry of the study area (lower). $S_o//S_1$ foliation (red lines), boudinaged quartz veins (L_1, blue polygons and lines), and S_2 foliation (dashed black lines). For scale, cobble markers on the tape measure are 1 meter apart, as are yellow painted lines from the measuring tape.

2.3.4 D_3 Structures

Locally S_o, S_1, and S_2 are buckled, forming 5-10cm wide kink bands (Figure 2-6e). The plunge of the F_3 kink folds is near vertical and the strike of axial planar kink bands (S_3) is NW-SE (Figure 2-8d).

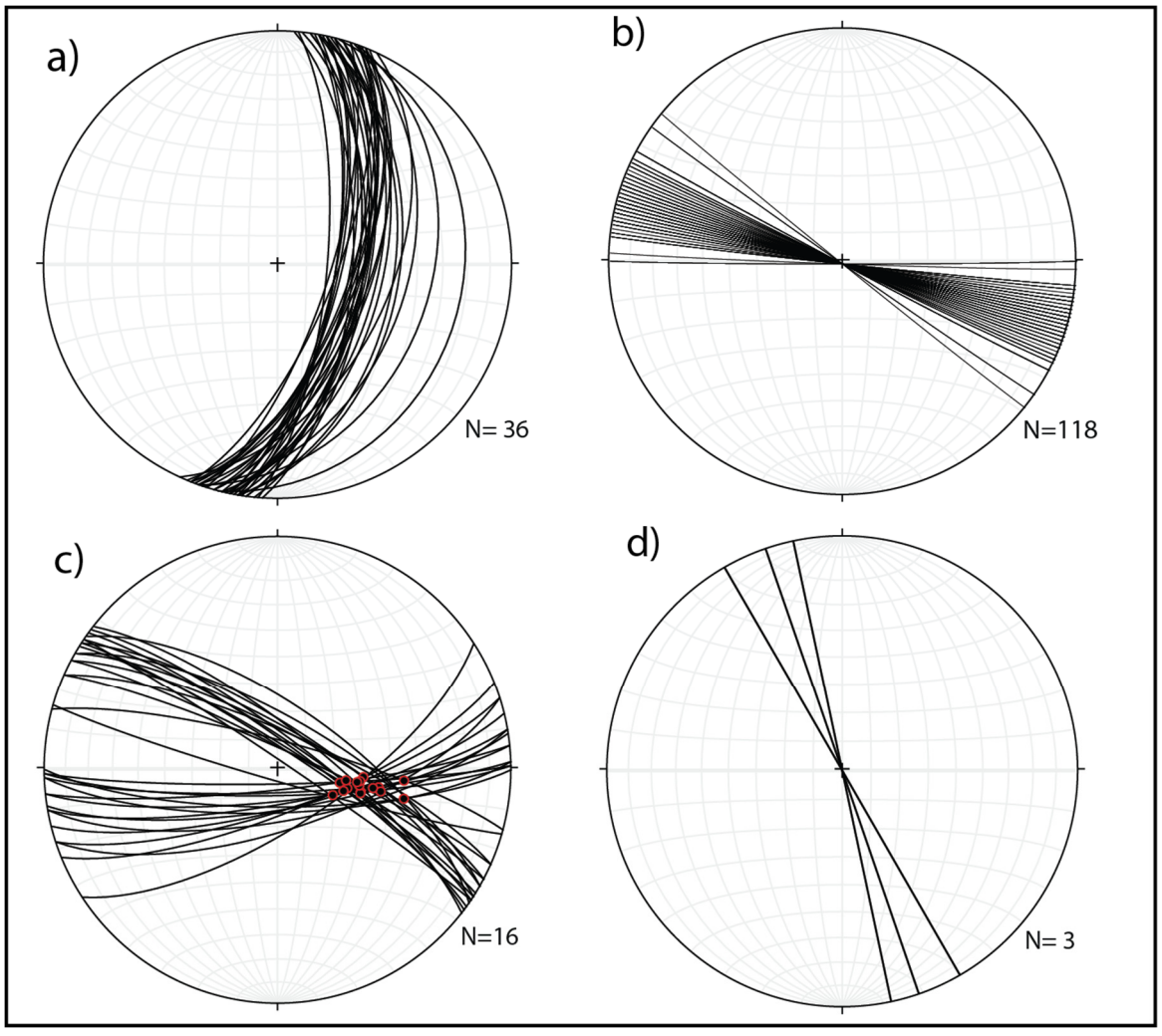

Figure 2-8 Stereonet of plotted data from Himanka. a) The ~N-S to NNE striking S_1 measured in F_2 hinge regions. b) WNW-ESE striking sub-vertical S_2 foliation. c) Steeply east plunging, tight to isoclinal F_2 fold geometry. F_2 fold limbs (great circles) and F_2 fold axes (red dots). d) NW-SE striking S_3 axial planes.

2.3.5 Summary

Isoclinal folding during D_1 is interpreted as recording dominantly pure shear (coaxial) deformation. The original orientation of $S_o//S_1$ prior to D_2 is speculative; previous studies hypothesize a NW-SE striking orogen and associated D_1 structures (Lahtinen et al., 2014). I make the assumption that the ~N to ~NNE striking S_1 preserved in F_2 fold hinges provides a sense of the original orientation of S_1. Hence, $S_o//S_1$ is predicted to be originally ~N to ~NNE striking and subsequently transposed to its current NW striking position, implying a progressive switch to simple shear (non-coaxial) deformation at some point towards the end of D_1 and beginning of D_2. The initial manifestation of this transposition towards the NW is depicted in Figure 2-9a.

D_2 is characterized by progressive deformation, which initiates as pure shear and partitions to a dominantly simple shear regime. The F_2 fold trains are interpreted as a series of discrete shear zones comprised of shear related folds. The F_2 fold trains accommodate shear strain in the limb regions and shortening in the hinge regions during an inferred counter clockwise rotation (Figure 2-9b). When applying an overall sinistral sense of shear to F_2 fold trains, the relative shear across these discrete zones provides a mechanism for the formation of F_2 folds, and stretching and thinning of the limbs. Furthermore, during progressive counter clockwise rotation the area between discrete shear zones undergoes shortening, forming F_2 folds and the S_2 foliation (Figure 2-9b). The sub-parallel plunge of L_1 boudins and F_2 fold axes indicates that F_1 and F_2 are coaxial. F_3 kink folds are interpreted as developing through prolonged NW-directed sinistral shear. Therefore, I conclude that F_2 and F_3 folds record a progressive counter-clockwise rotation of the proposed N to NNE striking S_1 foliation (Figure 2-9).

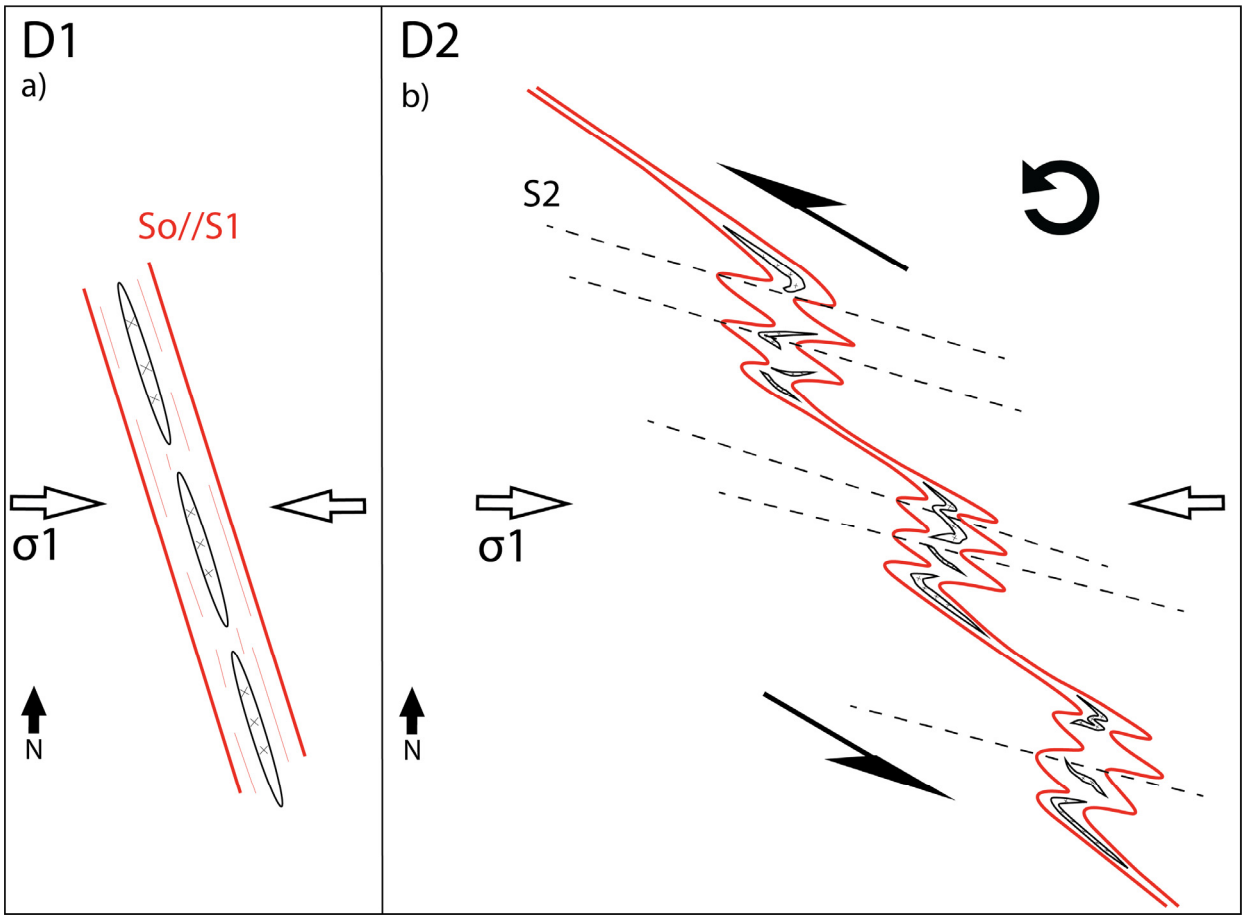

Figure 2-9 Progressive structural evolution in map view a) Steeply dipping NNW-SSE trending S_o//S_1 foliation and boudinaged dikes depicted prior to D_2 folding and early in the counter clockwise transposition of an originally N-S to NNE-SSW striking So//S_1 foliation. b) F_2 fold train geometry. Development of F_2 tight to isoclinal ESE plunging folds, sub-vertical, S_2 axial planar foliation. Folding and repositioning of boudins. Thinning and stretching of F_2 fold limbs recording sinistral shear and counter clockwise rotation. A fixed E-W compressive stress is proposed.

Structural analysis demonstrates that D_1, D_2, and D_3 structures stem from one protracted event where strain was initially accommodated by shortening (D_1), while becoming later partitioned into a larger component of simple shear (D_2 and D_3)(Figure 2-9). Assuming that the fold geometries developed in a simple shear regime, the inferred structural evolution can be explained as products of a constant or fixed E-W compressive stress (Figure 2-9). This interpretation implies that D_1, D_2, and D_3 events occurred in succession with little to no time gaps in between them. Given the similarities of folding style between the analysis herein and well documented D_1 and D_2 events in the Bothnian Arc

Complex (Rutland et al., 2001a; 2001b; Williams et al., 2008), I postulate that D_1, D_2, and D_3 events occurred during the Early Svecofennian Fennia event.

2.4 Metamorphism

The Svecofennian Orogenic Domain is characterized by high-temperature/ low-pressure mineral assemblages. Here, metamorphic textures (Figure 2-10) in the amphibolite-grade, meta-psammites and pelites are described and used to establish relative growth between porphyroblasts and their relationships with foliation sets.

2.4.1 Garnet

Garnets are common, forming 1-2mm wide, subhedral to euhedral porphyroblasts with internal inclusion trails (S_i) of quartz + plagioclase. The S_i inclusion trails are typically straight and are semi-continuous with an external (S_e) biotite foliation that exhibits sigmoidal geometry in garnet pressure shadows (Figure 2-10a, b). Hence, S_i and the S_e matrix counterpart are interpreted as S_1, which was developed prior to being overgrown by garnet. Another distinct matrix foliation, interpreted as S_2, shows biotite deflected around garnet porphyroblasts and overprints S_1 (Figure 2-10a, b). The textural relationships indicate that garnet post-dates S_1. Garnet is inferred to have crystallized during the early stages of D_2 overlapping with incipient deformation of the pre-existing S_1 foliation (Zwart, 1962; Bell and Rubenach, 1983; Passchier et al., 1992; Passchier and Speck, 1994).

2.4.2 Staurolite

Staurolite crystals are skeletal and are mantled, and locally pseudomorphed by quartz + plagioclase + andalusite + cordierite aggregate porphyroblasts (Figure 2-10d, e). Pseudomorphed porphyroblasts of andalusite + cordierite exhibit deformed fish-shaped grain boundaries (Figure 2-10d, e) and are restricted to pelitic beds (Figure 2-6e). In the matrix, isoclinal F_2 microfolds strongly crenulate S_1 biotite and the S_2 biotite foliation is deflected around the pseudomorphed porphyroblasts (Figure 2-10d, e). The textures indicate that relic staurolite crystals were deformed during D_2, prior to being replaced by aggregate pseudomorphs. Staurolite is inferred to have crystallized during and after garnet growth and to represent syn-D_2 prograde metamorphism. The prograde assemblages constrain peak conditions between the staurolite-in and -out reaction boundaries (reactions 4 and 5, Figure 2-11a petrogenetic grid) to temperatures between 500-575˚C and pressures above 3 kbar. Andalusite + cordierite replacement of staurolite is discussed in the following section.

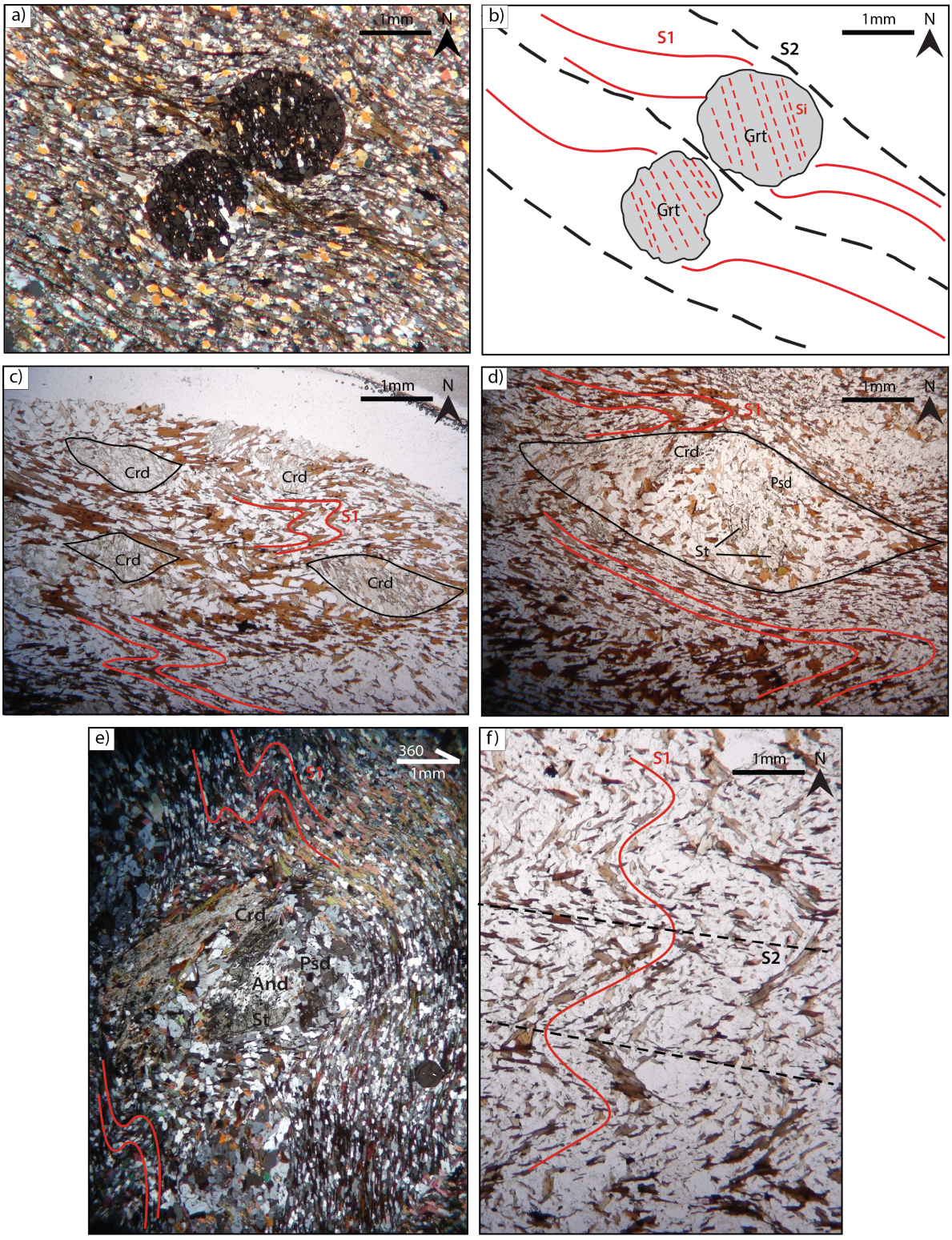

Figure 2-10 Photomicrographs of thin sections, oriented and cut perpendicular to biotite foliations. Red lines are F_2 micro-folds of S_o//S_1 foliations and dashed black lines are S_2 foliation. a) Microphotograph and annotation of garnet porphyroblasts and matrix foliations with internal garnet foliation S_i. Sample AB6, XPL, horizontal section. c) Fish shaped cordierite (Crd) porphyroblast with curved to sigmoidal poikiloblastic inclusions (S_i). Sample AB11, PPL, horizontal section. d) Fish shaped pseudomorph clast (Psd) aggregate of cordierite (Crd), quartz, plagioclase,

biotite and tourmaline after skeletal staurolite (St) porphyroblast. Sample GH8, PPL, horizontal section. e) Pseudomorph (Psd) clast of aggregate of cordierite (Crd), andalusite (And), quartz, plagioclase, and biotite after skeletal staurolite (St) porphyroblast. Sample VAB11, XPL, vertical section cut along N-S plane. f) S_0//S_1 foliation defined by aligned biotite grains and folded by F_2 micro-folds, S_2 axial planar cleavage is similarly defined by aligned biotite grains. Sample AB2, PPL, horizontal section.

2.4.3 Cordierite and Andalusite

Cordierite crystals are anhedral and commonly fish-shaped or disseminated throughout the matrix (Figure 2-10c). Cordierite is also found in the mantle rims of pseudomorphed staurolite (Figure 2-10d, e). In all cases, cordierite crystals have poikiloblastic inclusions of quartz and biotite, which in rare cases define sigmoidal trails (S_i). Andalusite occurs as a pseudomorph after staurolite and shares crystal boundaries with and is texturally controlled by skeletal staurolite crystals (Figure 2-10e). Cordierite and andalusite are inferred as the dominant post-deformational (post-D_{2-3}) phases and are coeval with aggregate pseudomorphs, which replace fish-shaped staurolite porphyroblasts that were deformed during D_2. My interpretation is supported by similar metamorphic textures observed in the Pohjanmaa Belt (Savunen, unpublished data, 2015; Hölttä and Heilimo, 2017, Fig 33a).

Assemblages of muscovite + staurolite + cordierite + biotite are not stable in meta-pelites (Pattison et al., 1999). Rocks that host these assemblages are inferred to be the result of two decompression reactions that follow a single P/T path (assemblage C, reaction 6 and 7, Figure 2-11b).

1) Ms + St + Qz = And + Bt + H_2O (reaction 6)

2) And + Bt + Qz + H_2O = Ms + Crd (reaction 7)

The first reaction produces andalusite after staurolite and the second produces cordierite after andalusite. The suggested breakdown reactions (Pattison et al., 1999) correspond to

the decompression textures observed in metamorphic assemblages (Figure 2-10c, d, e). Therefore, I interpret that post-deformational staurolite breakdown to cordierite and andalusite at Himanka is characteristic of isothermal decompression. The magnitude of decompression can be constrained by a decrease in pressure to below 3 kbar, which follows along the staurolite-out reaction boundary towards the cordierite-in reaction boundary (reaction 5 and 6 respectively, Figure 2-11a).

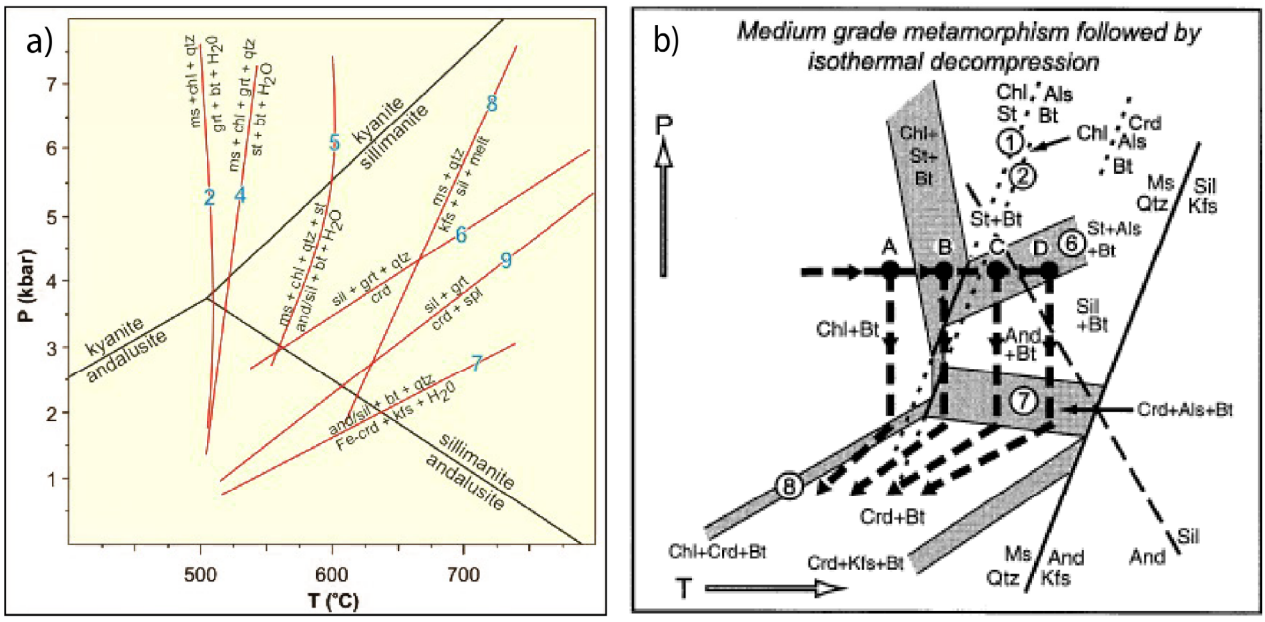

Figure 2-11 a) Petrogenetic grid showing major metamorphic reactions. Modified after Bucher & Frey (1994). b) Schematic P/T path modified after Pattison et al. (1999). Possible development of Ms+ Crd + St + Bt assemblages as a result of polymetamorphism. Paths A-D represent assemblages of Chl (A), St (B), St + And (C), and St + Sil (D).

2.5 U- Pb Monazite Geochronology

2.5.1 Sampling

A total 28 core samples were extracted in the field using a hand-held power drill with a 2.5 cm diameter diamond bit. All core samples were oriented towards north using a compass and any vertical discrepancies greater than 10 degrees were corrected for using a Pomeroy

orientation device. From the cores 25 horizontal and 8 vertical thin sections were prepared for SEM and LA-ICP-MS analysis. The majority of monazite grains were located in core samples taken from pelitic beds that also host metamorphic porphyroblasts of staurolite, andalusite and cordierite (Figure 2-6e). Monazite crystals are anhedral to euhedral and elongate to spherical. They occur as small (5-25μm) crystals that grow amongst quartz, plagioclase, and S_1 and S_2 biotite crystals in the matrix (Figure 2-12). Monazite often grow along the margins of, and in rare cases as inclusions within, the biotite crystals.

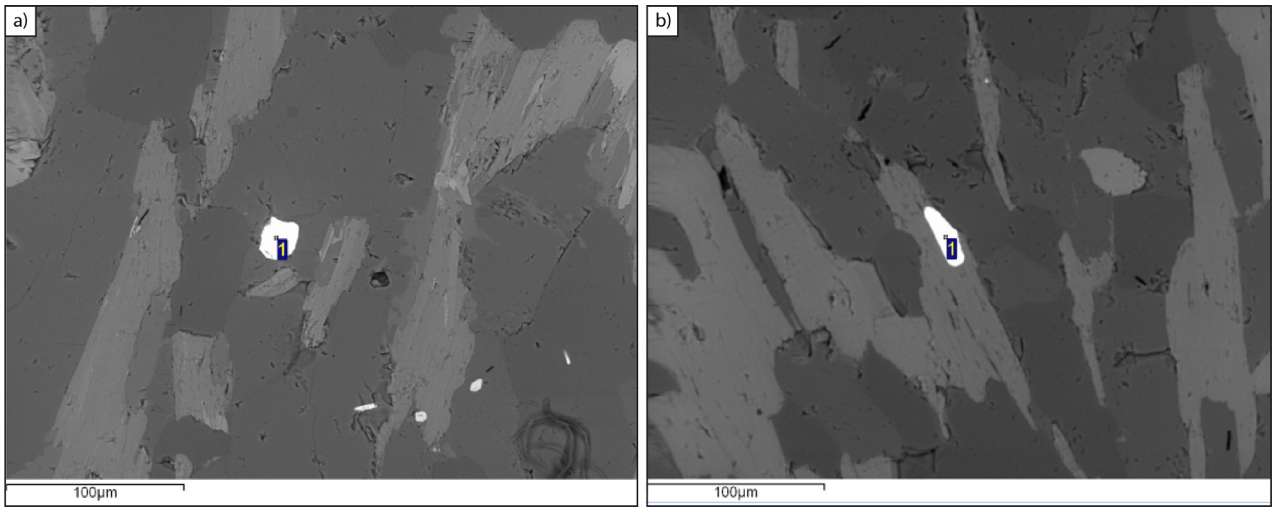

Figure 2-12 SEM images of textural variability of monazite a) GH6-1 and b) VAB11-7.

2.5.2 Analytical Methods

Thin sections were scanned using the scanning electron microscope (SEM) machine at the Geological Survey of Finland laboratory facilities. Monazites were identified by energy dispersive spectrometry (EDS) analysis (Scherrer et al., 2000). Other minerals rich in REE can be filtered out based on their brightness and the chemistry of their emission spectrum. The largest and best quality monazites were selected and mapped using a coordinate system

referenced to each thin section. U-Pb dating was performed on the LA-ICP-MS machine at the Geological Survey of Finland laboratory facilities, using methods described by Rosa et al. (2009). For the laser ablation procedure a 10 μm beam size, a 5 Hz repetition rate and an energy density of 3.32 J/cm^2 were used. The analysis was run using in house (Geological survey of Finland) monazite standards A49, A276, and A1326 for calibration and quality control.

The majority of monazite grains are small and/or narrow (short axis ≤10μm), and provide difficult targets for a 10μm beam size resulting in two limiting factors. First, other minerals bounding the monazites could have been ablated by the laser and incorporated into the analysis. Second, the laser could have overlapped significant features in the monazites, such as fractures or zoning. Isotope data was processed by Glitter data reduction software (Jackson et al., 2004). From 174 analyses there were 60 (34%) with high common Pb^{204} or high discordance that were discarded from the age calculations. All together there are good data from 114 analyses of 100 monazite grains. The U-Pb ages are calculated using ISOPLOT concordia diagram software. Apparent ages are given (Table 2-1a, b) with 2-sigma errors and 95% confidence.

Sample	Pb^{206}/Pb^{204}	Pb^{207}/Pb^{206}	2s%	Pb^{207}/U^{235}	2s%	Pb^{206}/U^{238}	2s%	% Concordance	age Pb^{207}/Pb^{206}	1s	age Pb^{207}/U^{235}	1s	age Pb^{206}/U^{238}	1s
GH5-1a	6017.00	0.11	2.12	5.22	2.22	0.34	2.15	-2.03	1839.06	19.04	1856.01	9.42	1870.77	17.43
GH5-2a	7713.11	0.11	2.34	4.97	2.47	0.32	2.24	2.35	1834.55	21.01	1814.35	10.39	1796.86	17.54
GH5-3a	-102014.82	0.11	2.41	4.88	2.54	0.32	2.25	0.41	1803.20	21.78	1799.23	10.64	1795.68	17.64
GH5-3b	3393.61	0.11	2.50	4.92	2.63	0.32	2.28	-0.22	1803.70	22.59	1805.06	11.04	1806.07	17.90
GH5-3c	3409.01	0.11	2.47	5.02	2.60	0.33	2.27	-2.76	1798.74	22.34	1821.90	10.94	1842.06	18.19
GH5-4b	8921.90	0.11	2.51	4.88	2.64	0.32	2.29	0.13	1801.06	22.63	1799.45	11.07	1797.83	17.92
GH5-9a	10442.53	0.11	2.63	4.95	2.78	0.32	2.36	0.45	1815.69	23.70	1811.39	11.68	1807.68	18.58
GH5-9b	4649.11	0.11	2.64	4.90	2.80	0.32	2.37	4.24	1837.13	23.68	1801.46	11.74	1770.90	18.29
AB11-1	3934.75	0.11	2.91	4.90	3.08	0.32	2.45	-0.64	1796.92	26.28	1801.86	12.90	1806.99	19.26
AB11-3	20053.16	0.11	2.87	4.82	3.05	0.32	2.45	0.27	1790.44	25.90	1787.67	12.74	1786.41	19.08
AB11-4	8116.82	0.11	3.06	4.84	3.23	0.32	2.45	-2.51	1771.35	27.72	1792.21	13.51	1810.06	19.30
AB11-5	7308.23	0.11	2.92	4.91	3.10	0.33	2.47	-5.70	1755.59	26.51	1804.34	12.99	1848.26	19.81
AB11-7a	635190.55	0.11	3.11	4.89	3.32	0.32	2.55	-1.48	1788.95	28.05	1800.97	13.90	1813.03	20.11
AB11-7b	5487.59	0.11	2.96	4.87	3.14	0.33	2.49	-3.31	1768.82	26.77	1796.61	13.15	1822.46	19.70
AB11-10a	5917.87	0.11	3.13	4.74	3.35	0.32	2.56	1.35	1786.61	28.26	1774.89	13.96	1765.85	19.77
AB11-10b	2793.39	0.11	2.97	5.04	3.18	0.33	2.51	-2.32	1806.83	26.75	1826.14	13.39	1845.45	20.11
AB11-11a	4220.63	0.12	3.14	5.14	3.32	0.32	2.50	4.81	1883.33	28.03	1842.72	14.02	1809.33	19.69
AB11-11b	18445.45	0.11	2.77	4.81	3.00	0.32	2.46	2.15	1805.02	25.00	1786.63	12.54	1772.37	19.07
EF4-1	-32914.76	0.11	3.01	4.85	3.24	0.32	2.53	-1.04	1785.28	27.14	1793.59	13.53	1803.24	19.90
EF4-9	14295.03	0.11	2.83	4.91	3.08	0.32	2.50	2.54	1825.15	25.47	1803.44	12.90	1787.63	19.51
GH6-1	3418.74	0.12	2.97	5.19	3.24	0.33	2.57	3.35	1880.20	26.55	1851.54	13.69	1829.80	20.40
GH6-2	3635.78	0.11	3.32	4.89	3.55	0.32	2.63	5.45	1845.17	29.69	1799.71	14.85	1765.51	20.31
GH6-3	3253.68	0.11	3.06	5.13	3.31	0.33	2.57	1.20	1851.09	27.38	1840.40	13.97	1834.55	20.48
GH6-8	11187.98	0.11	3.42	4.86	3.68	0.32	2.68	4.07	1829.21	30.65	1794.99	15.36	1771.78	20.73
GH7-2	-216122.92	0.11	2.24	5.07	2.36	0.34	2.17	-5.78	1781.10	20.29	1830.87	9.96	1874.78	17.66
GH7-5a	15783.60	0.11	2.30	5.20	2.40	0.34	2.19	-1.94	1836.48	20.67	1852.65	10.16	1866.92	17.69
GH7-6a	9470.21	0.11	2.29	5.07	2.40	0.33	2.18	-3.78	1798.74	20.71	1830.80	10.14	1859.04	17.61
GH7-6b	20135.02	0.11	2.29	5.01	2.39	0.33	2.18	-2.36	1801.22	20.67	1820.94	10.07	1838.04	17.43
GH7-8	47411.33	0.11	2.28	4.99	2.39	0.33	2.19	-1.54	1805.67	20.61	1818.33	10.06	1829.21	17.40
GH7-9a	-269883.67	0.11	2.26	5.13	2.37	0.34	2.19	-3.42	1811.43	20.37	1840.43	10.02	1866.09	17.69
GH7-9b	5036.89	0.11	2.24	5.16	2.36	0.34	2.18	-2.28	1826.93	20.16	1846.00	9.97	1862.81	17.65
GH7-1a	12395.17	0.11	2.30	5.07	2.42	0.33	2.20	-1.32	1820.26	20.73	1831.00	10.21	1840.42	17.56
GH7-1b	4614.39	0.11	2.32	5.23	2.43	0.34	2.20	-3.16	1830.50	20.91	1857.27	10.30	1881.18	17.93
GH8-3a	413871.00	0.11	2.31	4.96	2.42	0.33	2.20	-1.38	1800.73	20.84	1811.96	10.17	1821.69	17.42
GH8-3b	7832.67	0.11	2.30	5.03	2.41	0.33	2.20	-4.05	1789.61	20.83	1824.06	10.17	1854.31	17.67
GH8-4a	369898.00	0.11	2.33	5.04	2.44	0.33	2.20	-3.30	1797.58	21.05	1825.40	10.28	1849.86	17.68
GH8-4b	353939.00	0.11	2.32	4.96	2.42	0.33	2.20	-5.61	1764.59	21.02	1812.67	10.18	1854.70	17.72
GH8-6b	20097.42	0.11	2.29	4.85	2.41	0.33	2.20	-4.30	1757.81	20.78	1794.23	10.10	1825.67	17.46
GH8-7	19966.41	0.11	2.34	4.99	2.45	0.33	2.21	-1.50	1806.17	21.09	1818.40	10.31	1829.02	17.55
GH8-8	-26935.48	0.11	2.31	5.18	2.43	0.34	2.20	-4.16	1813.07	20.83	1848.59	10.29	1880.27	17.94
GH9-2	4405.46	0.11	2.35	5.03	2.46	0.32	2.22	1.96	1841.15	21.08	1824.14	10.36	1809.28	17.46
GH9-3	36994.00	0.11	2.65	4.94	2.73	0.32	2.26	2.28	1828.72	23.81	1809.14	11.46	1792.22	17.65
GH9-1	44583.13	0.11	2.36	4.93	2.47	0.33	2.21	-0.99	1800.23	21.34	1808.10	10.37	1814.88	17.49
GH9-6	-71512.48	0.11	2.33	4.87	2.44	0.33	2.21	-2.89	1772.36	21.07	1796.48	10.22	1817.26	17.48
GH9-7	-26884.34	0.11	2.34	4.82	2.46	0.32	2.22	-1.47	1777.24	21.17	1789.17	10.29	1799.49	17.38
GH9-8b	-863803.73	0.11	2.31	4.97	2.44	0.33	2.22	-2.31	1794.93	20.92	1814.13	10.25	1830.96	17.64
GH9-9a	253674.59	0.11	2.36	4.92	2.48	0.33	2.22	-7.35	1741.73	21.51	1805.21	10.40	1860.74	17.94
GH9-9b	433176.00	0.11	2.39	4.86	2.50	0.32	2.23	-0.35	1793.10	21.60	1795.57	10.48	1797.68	17.44
GH9-11	40807.31	0.11	2.37	4.99	2.48	0.33	2.22	-5.72	1768.15	21.47	1817.20	10.45	1860.35	17.94
GH11-1	-88849.49	0.11	2.48	4.83	2.58	0.32	2.25	-2.75	1767.30	22.48	1790.20	10.81	1810.01	17.70
GH11-2	10154.63	0.11	2.49	4.91	2.60	0.33	2.25	-1.86	1788.28	22.49	1803.64	10.90	1817.12	17.77
GH11-3a	10130.27	0.11	2.43	4.94	2.55	0.32	2.24	2.49	1829.85	21.88	1808.51	10.70	1790.27	17.51
GH11-3b	3968.56	0.11	2.50	4.94	2.60	0.32	2.25	4.25	1845.17	22.44	1809.39	10.93	1778.63	17.44
GH11-8	14285.71	0.11	2.54	4.79	2.64	0.32	2.26	-3.84	1750.13	23.07	1782.45	11.02	1810.50	17.79
GH11-10	-28117.40	0.11	2.49	4.73	2.60	0.32	2.25	-1.59	1759.51	22.59	1772.47	10.82	1783.82	17.52

Table 2-1a U-Pb isotopic LA-ICP-MS data of monazites from horizontal thin sections in the Pohjanmaa schist at Himanka.

Sample	Pb^{206}/Pb^{204}	Pb^{207}/Pb^{206}	2s%	Pb^{207}/U^{235}	2s%	Pb^{206}/U^{238}	2s%	% Concordance	age Pb^{207}/Pb^{206}	1s	age Pb^{207}/U^{235}	1s	age Pb^{206}/U^{238}	1s
GH11-11	4455.09	0.11	2.52	4.77	2.62	0.33	2.26	-4.90	1738.63	22.91	1780.19	10.96	1816.14	17.83
VAB11-5	-156142.41	0.11	2.12	4.87	2.15	0.32	2.06	0.58	1802.54	19.19	1797.17	9.02	1791.98	16.09
VAB11-7	515983.00	0.11	2.18	4.85	2.22	0.32	2.08	2.53	1814.87	19.68	1793.34	9.29	1774.28	16.09
VAB11-8	-33535.42	0.11	2.14	4.85	2.17	0.32	2.07	3.07	1819.77	19.29	1793.79	9.10	1770.90	16.00
VAB11-9	307014.50	0.11	2.11	4.77	2.16	0.31	2.07	4.23	1814.87	19.03	1779.44	9.02	1748.77	15.86
VAB11-10	10131.82	0.11	2.16	4.83	2.19	0.32	2.08	1.62	1803.53	19.50	1789.47	9.18	1776.87	16.13
VAB11-11	-57550.77	0.11	2.15	4.76	2.20	0.31	2.08	3.96	1811.43	19.40	1778.21	9.19	1749.46	15.90
VAB11-12a	1389216.32	0.11	2.19	4.82	2.25	0.32	2.10	1.71	1804.03	19.82	1789.23	9.40	1776.09	16.28
VAB11-12b	76987.79	0.11	2.20	4.79	2.26	0.32	2.11	1.75	1798.24	19.90	1783.20	9.44	1769.82	16.29
VAB11-14b	214599.00	0.11	2.28	4.94	2.34	0.32	2.13	-0.42	1806.66	20.60	1809.76	9.83	1811.86	16.77
VAB11-15	221197.00	0.11	2.17	4.84	2.24	0.32	2.11	2.01	1808.64	19.60	1791.36	9.38	1776.09	16.37
VAB11-16	-17019.54	0.11	2.20	4.88	2.27	0.32	2.12	1.71	1813.07	19.86	1798.27	9.53	1784.99	16.50
VAB11-18	-12687.92	0.11	2.18	4.79	2.26	0.31	2.12	4.17	1818.47	19.63	1783.54	9.45	1753.39	16.24
VEF4-1a	389044.00	0.11	2.25	4.96	2.33	0.33	2.14	-0.74	1806.17	20.28	1811.96	9.80	1816.44	16.95
VEF4-3b	-10339.70	0.11	2.28	4.98	2.37	0.33	2.16	-4.37	1779.25	20.65	1816.38	9.98	1848.46	17.35
VEF4-4b	361360.00	0.11	2.23	4.72	2.34	0.31	2.16	2.12	1789.61	20.18	1771.54	9.77	1755.75	16.57
VEF4-5	4867.36	0.11	2.56	4.71	2.64	0.32	2.21	-0.61	1763.75	23.20	1768.40	11.00	1771.78	17.07
VEF4-6a	244995.00	0.11	2.40	5.01	2.49	0.33	2.19	0.52	1825.31	21.62	1820.40	10.48	1815.61	17.29
VEF4-6b	-622103.69	0.11	2.31	4.94	2.42	0.33	2.18	-1.08	1800.23	20.85	1808.89	10.18	1815.85	17.24
VEF4-7	256043.00	0.11	2.34	4.96	2.44	0.32	2.19	0.96	1820.75	21.05	1812.19	10.24	1804.22	17.18
VEF4-8	-40280.89	0.11	2.37	5.01	2.50	0.33	2.21	-0.13	1821.08	21.36	1821.69	10.53	1821.59	17.52
VEF4-9	127132.39	0.11	2.33	4.80	2.47	0.32	2.21	0.00	1784.94	21.06	1784.46	10.31	1783.48	17.18
VEF4-10	6630.93	0.11	2.39	5.07	2.52	0.33	2.22	-1.19	1820.75	21.53	1830.36	10.62	1838.24	17.72
VEF4-11	11956.32	0.11	2.34	4.91	2.48	0.33	2.21	-5.22	1759.17	21.26	1803.69	10.40	1841.82	17.71
VEF4-12	-7074.18	0.11	2.39	4.89	2.52	0.33	2.22	-2.63	1779.42	21.64	1801.38	10.58	1819.74	17.57
VEF4-13	2322.31	0.11	2.50	5.01	2.62	0.33	2.24	-3.09	1794.60	22.56	1820.59	11.03	1842.69	17.95
VEF4-14	62912.20	0.11	2.30	4.96	2.45	0.33	2.21	-0.68	1806.99	20.75	1812.22	10.29	1816.10	17.49
VGH5-2a	50159.40	0.11	2.16	4.97	2.23	0.32	2.12	0.20	1817.16	19.48	1814.98	9.38	1812.69	16.72
VGH5-2b	3474.32	0.11	2.23	4.88	2.29	0.32	2.12	-0.64	1793.60	20.12	1798.51	9.58	1802.22	16.65
VGH5-4	5392.29	0.11	2.37	4.98	2.37	0.33	2.08	-3.86	1782.60	21.42	1815.24	9.95	1843.71	16.64
VGH5-6	-28969.63	0.11	2.12	4.92	2.16	0.33	2.08	-1.97	1789.11	19.20	1805.38	9.06	1819.16	16.46
VGH5-7	-19991.43	0.11	2.10	4.96	2.17	0.33	2.09	-2.55	1791.94	19.00	1813.20	9.11	1831.30	16.67
VGH5-8	20532.47	0.11	2.20	5.10	2.18	0.33	2.03	1.24	1846.45	19.74	1835.47	9.22	1826.01	16.10
VGH5-9	6596.21	0.11	2.17	4.92	2.25	0.33	2.13	-4.60	1767.30	19.64	1806.36	9.43	1839.93	16.99
VGH5-10	11222.77	0.11	2.18	4.84	2.19	0.32	2.05	2.49	1812.58	19.71	1791.37	9.17	1772.71	15.85
VGH5-11	7907.26	0.11	2.14	4.97	2.21	0.33	2.11	-1.61	1801.55	19.36	1814.74	9.30	1825.91	16.73
VGH5-13	3636.48	0.11	2.32	4.99	2.33	0.32	2.09	0.59	1822.71	20.86	1817.21	9.81	1812.30	16.48
VGH6-1	6434.67	0.11	2.17	4.86	2.30	0.32	2.19	1.80	1810.44	19.57	1794.93	9.64	1782.45	16.99
VGH6-4	15524.69	0.11	2.09	4.86	2.18	0.32	2.12	4.15	1830.34	18.83	1795.51	9.16	1765.56	16.35
VGH6-5	3531.89	0.11	2.25	4.94	2.30	0.31	2.12	6.39	1862.23	20.16	1809.18	9.65	1762.71	16.31
VGH6-6	14099.43	0.11	2.18	4.93	2.23	0.33	2.09	-6.47	1752.35	19.84	1808.00	9.37	1856.24	16.80
VGH6-9	38121.07	0.11	2.12	4.94	2.21	0.32	2.13	1.00	1818.14	19.15	1809.23	9.30	1801.49	16.70
VGH6-11	33214.78	0.11	2.18	4.93	2.25	0.32	2.11	-0.50	1804.19	19.65	1807.95	9.44	1810.79	16.63
VGH7-1	-65208.40	0.11	2.20	4.90	2.32	0.33	2.17	-4.11	1766.96	19.98	1801.70	9.74	1831.74	17.25
VGH7-4	11602.34	0.11	2.24	5.05	2.35	0.33	2.18	-0.34	1824.66	20.19	1827.06	9.92	1829.17	17.35
VGH7-5	6778.06	0.11	2.31	4.94	2.44	0.32	2.22	0.10	1810.94	20.86	1809.63	10.26	1808.70	17.46
VGH7-7	15904.88	0.11	2.37	4.93	2.49	0.33	2.21	-3.25	1780.59	21.45	1807.91	10.44	1831.69	17.59
VGH7-9	19493.28	0.11	2.29	4.99	2.43	0.32	2.21	2.91	1842.76	20.58	1817.91	10.22	1796.47	17.30
VGH7-11	24022.54	0.11	2.19	5.02	2.35	0.33	2.22	-0.03	1823.36	19.73	1823.13	9.90	1823.14	17.61
VGH7-13	-35675.44	0.11	2.36	4.78	2.47	0.32	2.20	0.83	1789.45	21.33	1782.05	10.33	1775.50	17.06
VGH7-14	15278.65	0.11	2.27	5.04	2.42	0.33	2.22	-2.58	1804.52	20.46	1826.15	10.19	1845.65	17.79
VGH8-1a	9607.73	0.11	2.22	4.95	2.37	0.33	2.20	-1.58	1797.91	20.06	1810.88	9.98	1822.32	17.47
VGH8-2	11859.26	0.11	2.27	5.11	2.45	0.33	2.25	1.99	1854.92	20.41	1837.65	10.35	1822.90	17.81
VGH8-3	-34407.15	0.11	2.44	4.98	2.60	0.33	2.26	-5.79	1765.95	22.16	1815.64	10.94	1859.29	18.19
VGH8-7	145608.47	0.11	2.26	4.91	2.43	0.33	2.24	-2.65	1781.60	20.45	1803.69	10.21	1823.05	17.76
VGH8-8	9712.88	0.11	2.23	4.93	2.42	0.33	2.25	-3.60	1776.90	20.18	1807.28	10.16	1833.97	17.92
VGH8-9	22232.77	0.11	2.33	5.02	2.51	0.33	2.26	-2.67	1799.57	21.02	1821.91	10.56	1842.02	18.09
VGH8-12	105869.00	0.11	2.23	5.07	2.42	0.34	2.26	-4.77	1790.78	20.16	1831.60	10.22	1867.98	18.26
VGH8-13	62631.30	0.11	2.27	4.97	2.46	0.33	2.25	-3.32	1786.95	20.54	1814.88	10.36	1839.59	18.00

Table 2-1b U-Pb isotopic LA-ICP-MS data of monazites from vertical thin sections in the Pohjanmaa schist at Himanka.

2.5.3 Results

The results of my LA-ICP-MS analysis of monazites (Table 2-1a, b) are shown on a concordia plot, which provides an age for the population at 1.80 Ga +/- 4.8 Ma (Figure 2-13). The age is calculated from the intercept of the regression line with concordia and the error of (+/-) 4.8 Ma is calculated from the intercept without decay-constant errors (Figure 2-13). When plotted on probability density plots (Figure 2-14), the monazite data show ages centered approximately at ~1.80 Ga for $^{207}Pb/^{206}Pb$, ~1.81 for $^{207}Pb/^{235}U$, and ~1.81 for $^{206}Pb/^{238}U$. However, the age ranges vary +/- 40-60 Ma. Therefore, my U-Pb analysis indicates that the majority of monazite grains crystallize at approximately ~1.80 Ga +/- 4.8 Ma (Figure 2-13), and that the range of monazites spans most of the late Svecofennian.

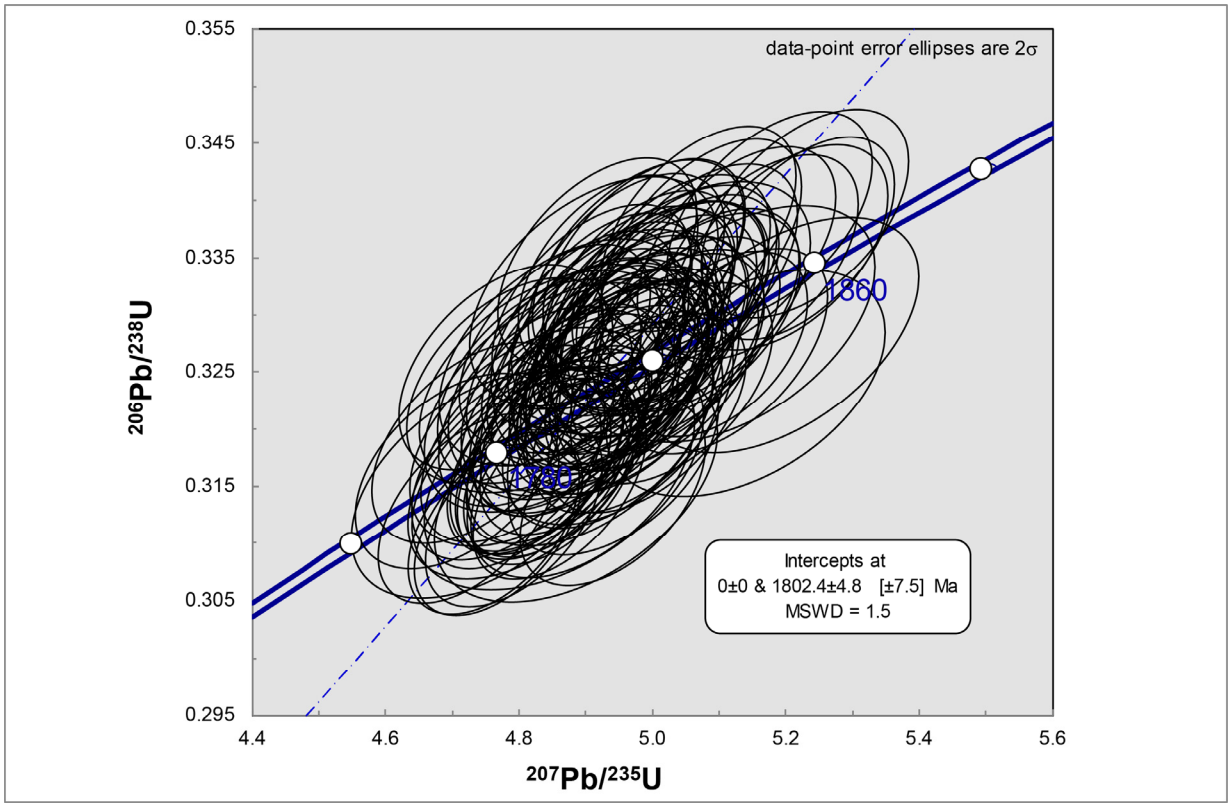

Figure 2-13 Concordia plot of 114 monazite grains shows a single population with an age of 1.80 Ga (+/- 4.8 Ma). The error of [+/-7.5] Ma is with decay constant errors.

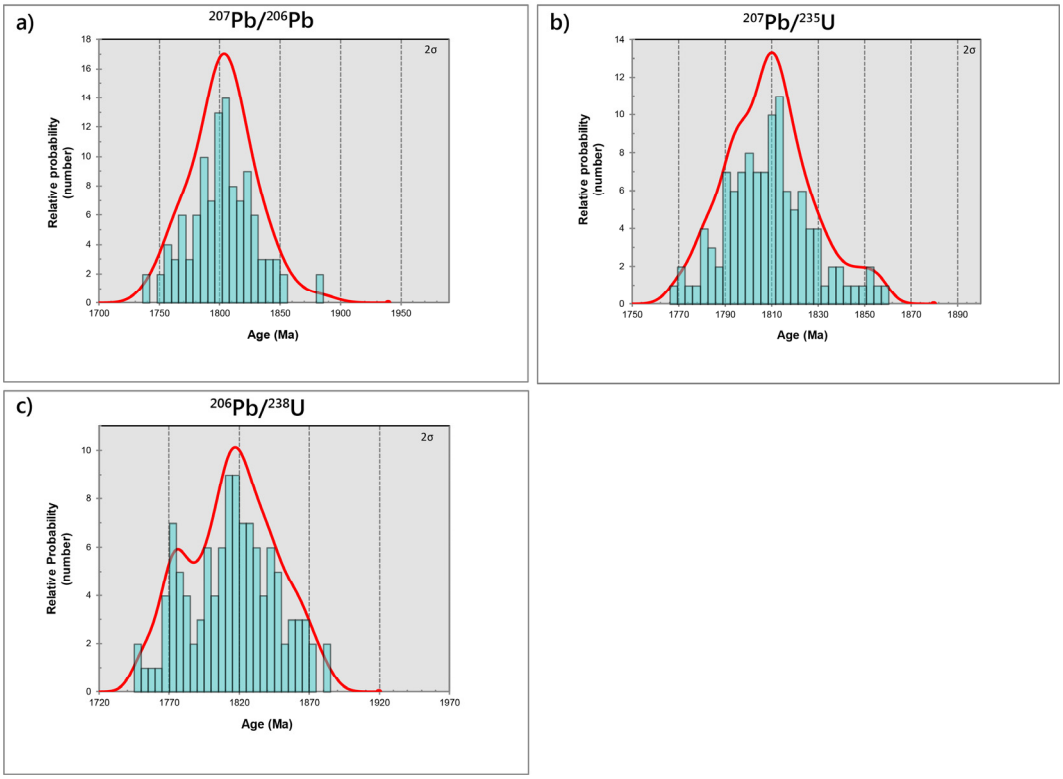

Figure 2-14 Probability density plots of the 114 monazite age data for each a) $^{207}Pb/^{206}Pb$, b) $^{207}Pb/^{235}U$, and c) $^{206}Pb/^{238}U$ systems. Plotted in bins of 40, with 2-sigma input errors.

2.6 Discussion

2.6.1 Timing of tectonothermal events

In my relative time-scheme two major tectonothermal events are identified at Himanka. D_2 is characterized by steeply ESE plunging F_2 fold trains, an ESE–WNW striking axial planar S_2 foliation, and coeval garnet + staurolite prograde metamorphism. Williams et al. (2008) identify ESE-WNW to NW-SE trending D_2 shear zones and folds that deform 1.896 Ga granitoids in the Himanka area. In their model they further constrain D_2 by peak metamorphic zircon ages to 1.88 Ga. I suggest that my D_2 deformation matches the structural style outlined by Williams et al., (2008) and correlates with well documented

deformation and metamorphism in the Pohjanmaa Belt during the early Svecofennian Fennia event from 1.896-1.88 Ga. The inferred direction of collision in the Bothnian Arc Complex during the early Svecofennian Fennia event is NE to ENE (Nironen, 1997; Lahtinen et al., 2009a; Lahtinen et al., 2014). However, my inferred progressive structural evolution suggests that D_1, D_2, and D_3 events (Figure 2-9) are products of a single protracted event and are most simply explained by fixed E-W compression. D_1 isoclinal folding and D_{2-3} shear related folds indicate partitioning from pure shear to simple shear deformation, which is likely the result of the counter clockwise rotation of the northern Pohjanmaa belt during the early Svecofennian Fennia event.

The late post-deformational tectonothermal event is characterized by staurolite breakdown to cordierite + andalusite pseudomorphs, which are suggested as products of isothermal decompression. It has been demonstrated that the P/T conditions during isothermal decompression and the related breakdown of staurolite to cordierite can be suitable for monazite growth (Gibson et al., 2004; Kelly et al., 2006; Mahan et al., 2006). This is the result of increased availability of REE and yttrium during the late-orogenic breakdown of garnet to cordierite. Monazite ages can be commonly be reset by younger metamorphic events, even below closure temperatures of 750-800˚C (Williams et al., 2007). Hence, it could be expected that the small monazites herein record the youngest metamorphic event. The monazite data herein plots on the concordia diagram with mostly overlapping error ellipses and are interpreted as a single U-Pb age population in the concordia diagram (Figure 2-13). Therefore, I interpret the 1.80 Ga (+/- 4.8 Ma) U-Pb monazite ages as recording the absolute timing of a post-deformational thermal event characterized by isothermal decompression. My interpretation is supported by similar, 1.80-1.79 Ga metamorphic

monazite ages from the Pohjanmaa Belt (Savunen, unpublished data, 2015). It appears that monazites provide an absolute age for a late thermal event that occurs 80-90 m. y. after D_2 and is not preserved in previously analyzed zircons. This implies that the 1.80 Ga tectonothermal event occurred towards the end of the late Svecofennian event.

Gravitational collapse has been argued to explain the high thermal signature and increased magmatism at the end of the late Svecofennian Svecobaltic event. Collisional processes during the early Fennia and the late Svecobaltic events can be modeled as having resulted in a thick and gravitationally unstable lithospheric root that subsequently delaminated, facilitating the rise of hot asthenosphere to the base of the crust (Nironen, 1997; Korsman et al., 1999; Korja et al., 2006). Delamination and thus thinning of the lower crust would provide a mechanism for an increased geothermal gradient and a decrease in pressure that could explain post-deformational high temperature /low pressure metamorphism and the strong magmatic pulse during the late Svecofennian event (Claesson and Lundqvist, 1995; Vaisanen and Hölttä, 1999; Vaisanen et al., 2002; Mouri et al., 2005; Skytta and Manttari, 2008; Torvela et al., 2008). Therefore, I postulate that the 1.80 Ga isothermal decompression textures provide a record of crustal thinning as a result of delamination and replacement of the lower crust 80-90 m. y. after the main D_2 event.

2.6.2 The coupled Bothnian oroclines

The coupled Bothnian oroclines are defined by sinuous lithotectonic belts, which are paralleled by structural fabrics. F_2 and F_3 folds in the study area record sinistral shear and their respective WNW and NW-striking axial traces are sub-parallel to the local margin of the Pohjanmaa Belt, which is inferred to form the northern limb of the convex to the east

northern member of the coupled Bothnian Oroclines. Similarly, the strike of F_2 folds sub-parallel the margins of the southern Pohjanmaa Belt (Bothnian Arc Complex), which together bend around the southern Bothnian orocline from N-S in the hinge to E-W in the shared limb between the north and south Bothnian oroclines (Lehtonen et al., 2005; Lahtinen et al., 2017). However in this region, folds record an inferred dextral sense of shear and an implied clockwise rotation in the southern limb of the northern Bothnian orocline (S. Johnston, unpublished data, 2014). The sense of shear during F_2 and F_3 folding is, therefore, a function of location with respect to the hinge lines of the Bothnian oroclines: F_2 and F_3 record sinistral shear along the northern limb of the northern orocline, and dextral shear along the intermediate shared limb (Figure 2-15). This implies that F_2 and F_3 folds are pre- to syn-oroclinal. Further evidence to support this relationship is the trace of early Svecofennian metamorphic isograds, which subparallel the sinuous belts around the oroclines (Lahtinen et al., 2014; Hölttä and Heilimo, 2017).

My findings are consistent with the Svecofennian orogen having originated as a roughly linear ~N-S (this study) to NW-SE (Lahtinen et al., 2014) striking belt that was subsequently deformed into its current sinuous geometry. In their model Lahtinen et al. (2014) propose that the formation of the coupled Bothnian oroclines is secondary and resulted from a near-orthogonal switch in compressive stress. However, my data and analysis shows that deformation (D_1 through D_3) was progressive and synchronous with counter clockwise rotation and sinistral shear of the northern Pohjanmaa Belt during orocline formation (Figure 2-15). Hence, I conclude that the coupled Bothnian oroclines are a product of progressive bending during orogenesis. A model of progressive bending is consistent with shear being a function of location on the orocline limbs, and implies that, the

oroclines are a product of the 1.896-1.88 Ga early Svecofennian Fennia event.

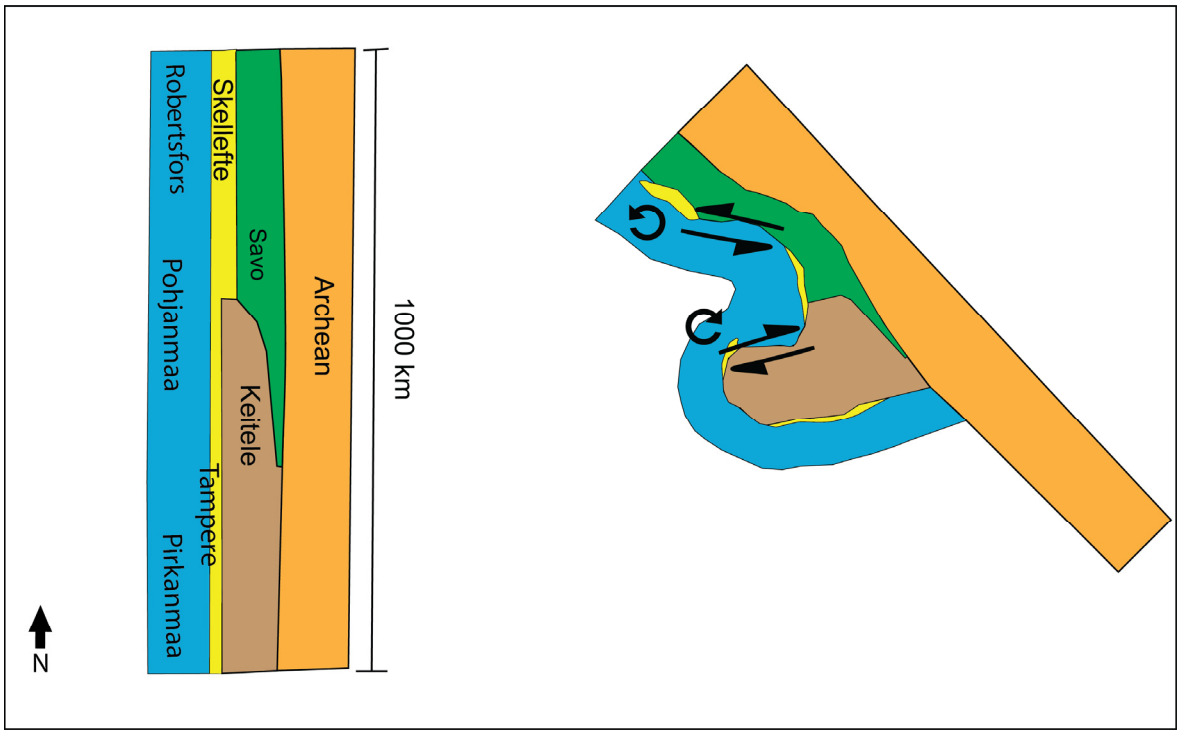

Figure 2-15 Schematic showing the model for buckling of a hypothesized ~N-S linear Svecofennian orogen to form the arcuate coupled Bothnian oroclines. The northern Bothnian orocline (convex-east) showing sinistral shear in the north limb and dextral shear in the south limb with the respective counter clockwise and clockwise implied rotations. Modified from Lahtinen et al. (2014).

High temperature - low pressure metamorphism at 1.80 Ga is explained as a result of late Svecofennian Svecobaltic delamination of mantle and lower crust that was previously thickened during the early Svecofennian Fennia event. The implication is that the upper crust remained coupled to the lower crust and mantle during early Svecofennian Fennia event compression and orocline formation. Hence, I conclude that orocline formation was thick-skinned and involved the lithospheric mantle. What remains unclear is if thickening, and subsequent detachment, of the lithospheric mantle was a product of the collisional orogeny or if it was product of oroclinal bending. Studies by Gutiérrez-Alonso et al. (2004)

and Weil et al. (2013) suggest that oroclinal bending causes thickening of the inner orocline arc which leads to: 1) uplift and rapid sedimentation towards the forearc; 2) the initiation of crustal thinning and high heat flow and magmatism in the outer arc of the orocline; 3) subsequent delamination of the mantle lithosphere below a thickened orocline core causing wide-spread magmatism, fluid flow and high temperature / low pressure metamorphism in the inner arc of the orocline. It could be argued that the Bothnian oroclines meet these criteria; however, further testing of this model is required.

Johnston et al. (2013) interpreted progressive oroclines as being thin skinned features that required a detachment between the bending upper crust and the unaffected lower crust and lithospheric mantle. My findings are inconsistent with this classification scheme and require that the idea that oroclines can be readily classified as progressive or secondary be revisited.

2.7 Concluding Remarks

I investigated the structure, metamorphism, and geochronology of the Pohjanmaa Belt on the northern limb of the northern of the two coupled Bothnian oroclines in order to establish whether or not deformation is consistent with the Bothnian orocline model. Also, I attempt to provide relative and absolute time constraints on oroclinal buckling. My data show that: 1) D_1, D_2, D_3 deformation in the Pohjanmaa belt records progressive deformation and strain partitioning from pure shear (D_1 shortening) to simple shear (D_2, D_3 sinistral shear), which involved counter clockwise rotation and can possibly be explained by E-W directed compression; 2) D_2 folding and coeval garnet + staurolite metamorphism are consistent with early Svecofennian Fennia deformation, which occurred 80-90 m. y. prior to

late-stage isothermal decompression and staurolite breakdown dated at 1.80 Ga by U-Pb monazite analysis; 3) My structural analysis, in combination with subsidiary data, provides evidence that sinistral shear during $D_{2\text{-}3}$ is the result of counter clockwise rotation of the Pohjanmaa belt possibly in response to progressive buckling of the coupled Bothnian oroclines during the early Svecofennian Fennia event.

Chapter 3. Conclusions

3.1 Conclusions

The goal of this thesis was to evaluate the deformation and metamorphism of the northern limb of the northern Bothnian orocline to help establish the structures that may characterize orocline formation and provide an absolute constraint on the timing of buckling. I addressed this goal through detailed mapping of the fold geometry and assessment of metamorphic-textures in the meta-sedimentary Pohjanmaa belt in the Svecofennian Orogenic Domain. This allowed for me to develop a structural model and a relative time-scheme between deformation and metamorphism. My U-Pb analysis of monazite grains was used to constrain the timing of tectonothermal events in the northern of the two Bothnian oroclines. The main conclusions of this thesis are:

1) D_1, D_2, and D_3 studied herein record deformation from a single protracted event in which, strain was initially accommodated by pure shear (D_1 shortening) and was later partitioned to dominant components of simple shear (D_2 and D_3 sinistral shear). D_1, D_2, and D_3 are inferred as products of E-W directed compression during the early Svecofennian Fennia event.
2) Syn-D_2 prograde garnet + staurolite growth likely occurred during the well-documented early Svecofennian metamorphic event from 1.896-1.88 Ga.
3) The absolute timing of a late, post-deformational isothermal decompression event characterized by staurolite breakdown to cordierite + andalusite is provided by 1.80 Ga U-Pb isotope ages. Hence, the thermal signature is late Svecofennian and records crustal thinning as the result of gravitational collapse of an orogen.

4) The axial traces of F_2 and F_3 folds sub-parallel the margins of sinuous belts around the coupled Bothnian oroclines, indicating they are pre- to syn-oroclinal. My structural analysis suggests that sinistral shear during D_{2-3} records counter clockwise rotation of the Pohjanmaa Belt, which could be in response to buckling of the coupled Bothnian oroclines during the early Svecofennian Fennia event.
5) My findings are inconsistent with the classification of progressive oroclines as being exclusively thin skinned features that required a detachment between the bending upper crust and the unaffected lower crust and lithospheric mantle.

3.2 Recommendations for further work

Oroclines are complex tectonic features and even the most well studied oroclines are not completely understood. This thesis is one of the first few studies of the coupled Bothnian oroclines and one of the few studies that focuses specifically on Precambrian oroclines. As such, my findings come early on in the overall study of the coupled Bothnian oroclines and Precambrian oroclines in general. The findings herein reveal new research questions, which through further investigation will help develop the model of the coupled Bothnian oroclines and how it fits with the evolution of the Svecofennian Orogenic Domain.

My new structural data points to a test of the orocline model (Lahtinen et al., 2014). If sinistral shear during D_{2-3} was characteristic of the original orogen and occurred prior to oroclinal buckling, then I would expect it to be consistent around the orocline hinges. Conversely, if sinistral shear were the result of oroclinal buckling, then I would expect the sense of shear to change systematically from one limb to another, across the hinge of the orocline. A study carried out by Shaw et al. (2016) analyzed parasitic vertical-axis kink folds

along the strike of the Cantabrian orocline in Iberia. They determined that the kink folds verge towards the orocline hinge and record a switch in the sense of shear from each limb of the orocline, which they attribute to flexural shear during buckling. I propose that applying similar methods as Shaw et al. (2016) would be helpful in determining whether or not the inferred sinistral shear that gave rise to F_2 fold trains (Figure 2-9) and F_3 kink folds (Figure 2-6e) in the Pohjanmaa Belt could be a function of buckling of the coupled Bothnian oroclines or a characteristic of initial orogenesis. This could provide insight in discerning what structures could be diagnostic of orocline forming in hot deep crustal conditions.

The Bergslagen orocline of southern Sweden (Beunk and Kuipers, 2012) remains one of the few other examples of Paleoproterozoic oroclines. In their model, the convex to-the-NW geometry of the Bergslagen province is explained by buckling of D_2 structures during D_4 folding, which is activated along SW-NE striking shear zones and characterized by sinistral shear. Progressive rotation (D_4) of the Bergslagen province is suggested to have taken place during the late Svecofennian Svecobaltic event from 1.83-1.82 Ga and connections between large shears zones in Sweden and the Southern Svecofennian Arc Complex in Finland are implied. I propose further investigation of the similarities in deformation and timing between the Bergslagen and Bothnian oroclines. This could address the question, how the Svecofennian Orogenic Domain became characterized by multiple arcuate orogenic belts.

Monazites in pelitic rocks are interpreted to grow at the expense of garnet and other aluminous porphyroblasts (Smith and Barreiro, 1990; Pyle and Spear, 2003). As the breakdown of these mid- to high-grade porphyroblasts occurs the availability rare earth elements provides the building blocks for monazite crystallization. In particular, studies using elemental microprobe mapping of monazites suggest that late-orogenic monazite rims

are suggested to have high amounts of yttrium (Gibson et al., 2004; Kelly et al., 2006; Mahan et al., 2006). If continued U-Pb monazite analyses are used to study and date metamorphic events in the Svecofennian Orogenic Domain, I suggest that the incorporation of microprobe elemental mapping would be useful and possibly critical to determining: 1) whether or not monazites have internal chemical zones; 2) whether high-yttrium monazites or their rims provide consistent ages that can be tied to certain tectonothermal events.

References

Aerden, D.G.A.M., 2004, Correlating deformation in Variscan NW-Iberia using porphyroblasts; implications for the Ibero-Armorican Arc: Journal of Structural Geology, v. 26, no. 1, p. 177–196, doi: 10.1016/S0191-8141(03)00070-1.

Bell, T.H., and Rubenach, M.J., 1983, Sequential porphyroblast growth and crenulation cleavage development during progressive deformation: Tectonophysics, v. 92, no. 1–3, p. 171–194, doi: 10.1016/0040-1951(83)90089-6.

Beunk, F.F., and Kuipers, G., 2012, The Bergslagen ore province, Sweden: Review and update of an accreted orocline, 1.9-1.8Ga BP: Precambrian Research, v. 216–219, p. 95–119, doi: 10.1016/j.precamres.2012.05.007.

Bucher, K., & Frey, M., 1994, Metamorphism of Pelitic Rocks (Metapelites). In Petrogenesis of Metamorphic Rocks (pp. 191-232). Springer, Berlin, Heidelberg.

Cardozo, N., and Allmendinger, R.W., 2013, Spherical projections with OSXStereonet: Computers and Geosciences, v. 51, p. 193–205, doi: 10.1016/j.cageo.2012.07.021.

Carey, S.W., 1955, The orocline concept in geotectonics-Part I: Papers and proceedings of the Royal Society of Tasmania, v. 89, p. 255–288.

Chopin, F., Korja, A., Hölttä, P., Eklund, O., & Rämö, O. T., 2014. The Vaasa dome: its tectonic and metamorphic evolution during the Svecofennian orogeny. In Lithosphere 2014—Eighth Symposium on the Structure, Composition and Evolution of the Lithosphere in Finland. Programme and Extended Abstracts, Turku, Finland (pp. 9-12).

Claesson, S., and Lundqvist, T., 1995, Origins and ages of Proterozoic granitoids in the Bothnian Basin, central Sweden; isotopic and geochemical constraints: Lithos, v. 36, no. 2, p. 115–140, doi: 10.1016/0024-4937(95)00010-D.

Ehlers, C., Lindroos, A., and Selonen, O., 1993, The late Svecofennian granite-migmatite zone of southern Finland-a belt of transpressive deformation and granite emplacement: Precambrian Research, v. 64, no. 1–4, p. 295–309, doi: 10.1016/0301-9268(93)90083-E.

Eldredge, S., Bachtadse, V., and Van Der Voo, R., 1985, Paleomagnetism and the orocline hypothesis: Tectonophysics, v. 119, no. 1–4, p. 153–179, doi: 10.1016/0040-1951(85)90037-X.

Gaal, G., and Gorbatschev, R., 1987, An outline of the Precambrian evolution of the Baltic Shield: Precambrian Research, v. 35, p. 15–52.

Gibson, H.D., Carr, S.D., Brown, R.L., and Hamilton, M.A., 2004, Correlations between chemical and age domains in monazite, and metamorphic reactions involving major pelitic phases: An integration of ID-TIMS and SHRIMP geochronology with Y-Th-U X-ray

mapping: Chemical Geology, v. 211, no. 3–4, p. 237–260, doi: 10.1016/j.chemgeo.2004.06.028.

Del Greco, K., Johnston, S. T., Gutiérrez-Alonso, G., Shaw, J., & Lozano, J. F., 2016, Interference folding and orocline implications: A structural study of the Ponga Unit, Cantabrian orocline, northern Spain. Lithosphere, *8*(6), 757-768.

Gibson, H. D., Carr, S. D., Brown, R. L., & Hamilton, M. A., 2004, Correlations between chemical and age domains in monazite, and metamorphic reactions involving major pelitic phases: an integration of ID-TIMS and SHRIMP geochronology with Y–Th–U X-ray mapping. Chemical Geology, 211(3-4), 237-260.

Gutiérrez-Alonso, G., Fernández-Suárez, J., and Weil, A.B., 2004, Orocline triggered lithospheric delamination: Geological Society of America Special Papers, v. 383, no. 2, p. 121–130, doi: 10.1130/0-8137-2383-3(2004)383[121:otld]2.0.co;2.

Hölttö, P., and Heilimo, E., 2017, Metamorphic Map of Finland: Geological Survey of Finland, Special Papper, no. 60, p. 75–126.

Jackson, S.E., Pearson, N.J., Griffin, W.L., and Belousova, E.A., 2004, The application of laser ablation-inductively coupled plasma-mass spectrometry to in situ U-Pb zircon geochronology: Chemical Geology, v. 211, no. 1–2, p. 47–69, doi: 10.1016/j.chemgeo.2004.06.017.

Johnston, S.T., 2001, The Great Alaskan Terrane Wreck: Reconciliation of paleomagnetic and geological data in the Northern Cordillera: Earth and Planetary Science Letters, v. 193, no. 3–4, p. 259–272, doi: 10.1016/S0012-821X(01)00516-7.

Johnston, S.T., Weil, A.B., and Gutiérrez-Alonso, G., 2013, Oroclines : Thick and thin. Bulletin, no. 5, p. 643–663, doi: 10.1130/B30765.1.

Kelly, N.M., Clarke, G.L., and Harley, S.L., 2006, Monazite behaviour and age significance in poly-metamorphic high-grade terrains : A case study from the western: v. 88, p. 100–134, doi: 10.1016/j.lithos.2005.08.007.

Kilpelainen, T., Korikovsky, S., Korsman, K., and Nironen, M., 1994, Tectono-Metamorphic Evolution in the Tampere-Vammala area: Geological Survey of Finland, v. Guide 37, no. Pajunen, M (ed.) High temperature-low pressure metamorphism and deep crustal structures., p. 27–34.

Kilpelainen, T., 1998, Evolution and 3D modeling of structural and metamorphic patterns of the Paleoproterozoic crust in the Tampere-Vammala area, southern Finland: Geological Survey of Finland, v. 397, no. Bulletin, p. 1–124.

Koistinen, T., Klein, V., Koppelmaa, H., Korsman., Lahtinen, R., Nironen, M., Puura, V., Saltykova, T., Tikhomirov, S., and Yanovskiy, A., 1996, Paleoproterozoic Svecofennian orogenic belt: Geological Survey of Finland, v. Koistinen, no. Special Paper 21, p. 21–57.

Korja, A., and Heikkinen, P., 2005, The accretionary Svecofennian orogen - Insight from the BABEL profiles: Precambrian Research, v. 136, no. 3–4, p. 241–268, doi: 10.1016/j.precamres.2004.10.007.

Korja, A., Lahtinen, R., and Nironen, M., 2006, The Svecofennian orogen: a collage of microcontinents and island arcs: Geological Society, London, Memoirs , v. 32, no. 1, p. 561–578, doi: 10.1144/GSL.MEM.2006.032.01.34.

Korsman, K., Korja, T., Pajunen, M., and Virransalo, P., 1999, The GGT/SVEKA Transect: Structure and Evolution of the Continental Crust in the Paleoproterozoic Svecofennian Orogen in Finland: International Geology Review, v. 41, no. 4, p. 287–333, doi: 10.1080/00206819909465144.

Lahtinen, R., 1997, Crustal evolution of the Svecofennian and Karelian domains during 2.1-1.79 Ga, with special emphasis on the geochemistry and origin of 1.93-1.91 Ga gneissic tonalites and associated supracrustal rocks in the Rautalampi area, central Finland.

Lahtinen, R., Huhma, H., and Kousa, J., 2002, Contrasting source components of the Paleoproterozoic Svecofennian metasediments: Detrital zircon U-Pb, Sm-Nd and geochemical data: Precambrian Research, v. 116, no. 1–2, p. 81–109, doi: 10.1016/S0301-9268(02)00018-9.

Lahtinen, R., Garde, A. a, and Melezhik, V. a, 2008, Paleoproterozoic evolution of Fennoscandia and Greenland: Episodes, v. 31, no. 1, p. 20–28.

Lahtinen, R., Huhma, H., Kahkonen, Y., and Manttari, I., 2009a, Paleoproterozoic sediment recycling during multiphase orogenic evolution in Fennoscandia, the Tampere and Pirkanmaa belts, Finland: Precambrian Research, v. 174, no. 3–4, p. 310–336, doi: 10.1016/j.precamres.2009.08.008.

Lahtinen, R., Korja, A., Nironen, M., and Heikkinen, P., 2009b, Paleoproterozoic accretionary processes in Fennoscandia: The Geological Society, London, Special Publications, v. 318, no. Cawood, P. A. & Kroner, A. (eds) Earth and Accretionary Systems in Space and Time., p. 237–256.

Lahtinen, R., Johnston, S.T., and Nironen, M., 2014, The Bothnian coupled oroclines of the Svecofennian Orogen: A Palaeoproterozoic terrane wreck: Terra Nova, v. 26, no. 4, p. 330–335, doi: 10.1111/ter.12107.

Lahtinen, R., Huhma, H., Sipilä, P., & Vaarma, M., 2017, Geochemistry, U-Pb geochronology and Sm-Nd data from the Paleoproterozoic Western Finland supersuite–A key component in the coupled Bothnian oroclines. Precambrian Research, 299, 264-281.

Lehtonen, M.I., Kujala, H., Kärkkäinen, N., Lehtonen, A., Mäkitie, H., Mänttäri, I., Virransalo, P., and Vuokko, J., 2005, Etelä-Pohjanmaan liuskealueen kallioperä.:

Lind, P.-D. 2013. Modelling P-T conditions in the Lappfors group of the Svecofennian,

Kokkola, SW Finland. Johannes Gutenberg-Universität, Mainz, Institut für Geowissenschaften, AG Metamorphe Geologie. 94 p. (unpublished MSc thesis)

Lundqvist, T., Vaasjoki, M., and Persson, P.-O., 1998, U–Pb ages of plutonic and volcanic rocks in the Svecofennian Bothnian Basin, central Sweden, and their implications for the Palaeoproterozoic evolution of the Basin: Gff, v. 120, no. November 2016, p. 357–363, doi: 10.1080/11035899801204357.

Mahan, K.H., Goncalves, P., Williams, M.L., and Jercinovic, M.J., 2006, Dating metamorphic reactions and fluid flow : application to exhumation of high- P granulites in a crustal-scale shear zone , western Canadian Shield: , p. 193–217, doi: 10.1111/j.1525-1314.2006.00633.x.

Mouri, H., Korsman, K., and Huhma, H., 1999, Tectono-Metamorphic evolution and timing of the melting processes in the Svecofennian tonalite-trondhjemite migmatite belt: And example from Luopionen, Tampere, southern Finland: Geological Society of Finland, v. 71, no. Bulletin, p. 31–56.

Mouri, H., Väisänen, M., Huhma, H., and Korsman, K., 2005, Sm–Nd garnet and U–Pb monazite dating of high-grade metamorphism and crustal melting in the West Uusimaa area, southern Finland: Gff, v. 127, no. 2, p. 123–128, doi: 10.1080/11035890501272123.

Nironen, M., 1989, The Tampere Schist Belt: structural style within an early Proterozoic volcanic arc system in southern Finland: Precambrian Research, v. 43, no. 1–2, p. 23–40, doi: 10.1016/0301-9268(89)90003-X.

Nironen, M., 1997, The Svecofennian Orogen: a tectonic model: Precambrian Research, v. 86, no. 86, p. 21–44, doi: 10.1016/S0301-9268(97)00039-9.

Nironen, M., Elliott, B.A., and Rämö, O.T., 2000, 1.88-1.87 Ga post-kinematic intrusions of the Central Finland Granitoid Complex: A shift from C-type to A-type magmatism during lithospheric convergence: Lithos, v. 53, no. 1, p. 37–58, doi: 10.1016/S0024-4937(00)00007-4.

Passchier, C., Trouw, R., Zwart, H., Vissers, R., 1992, Porphyroblast rotation: eppur si mouve? Journal of Metamorphic Geology, v. 10, p. 283–294.

Passchier, C.W., and Speck, P.J.H.R., 1994, The kinematic interpretation of obliquely-transected porphyroblasts: an example from the Trois Seigneurs Massif, France: Journal of Structural Geology, v. 16, no. 7, p. 971–984, doi: 10.1016/0191-8141(94)90079-5.

Pattison, D.R.M., Spear, F.S., and Cheney, J.T., 1999, Polymetamorphic origin of muscovite + cordierite + staurolite + biotite assemblages: Implications for the metapelitic petrogenetic grid and for P-T paths: Journal of Metamorphic Geology, v. 17, no. 6, p. 685–703, doi: 10.1046/j.1525-1314.1999.00225.x.

Pyle and Spear, 2003, Four generations of accessory-phase growth in low pressure

migmatite from NW New Hampshire: American Mineralogist, 88 (2-3), p.338-351,doi: 10.2138/am-2003-2-311

Rosa, D.R.N., Finch, a. a., Andersen, T., and Inverno, C.M.C., 2009, U–Pb geochronology and Hf isotope ratios of magmatic zircons from the Iberian Pyrite Belt: Mineralogy and Petrology, v. 95, p. 47–69, doi: 10.1007/s00710-008-0022-5.

Rutland, R.W.R., Kero, L., Nilsson, G., and Stolen, L.K., 2001a, Nature of a major tectonic discontinuity in the Svecofennian province of northern Sweden: Precambrian Research, v. 112, no. 3–4, p. 211–237, doi: 10.1016/S0301-9268(01)00165-6.

Rutland, R.W.R., Skiold, T., and Page, R.W., 2001b, Age of deformation episodes in the Palaeoproterozoic domain of northern Sweden, and evidence for a pre-1.9 Ga crustal layer: Precambrian Research, v. 112, no. 3–4, p. 239–259, doi: 10.1016/S0301-9268(01)00166-8.

Rutland, R.W.R., Williams, I.S., and Korsman, K., 2004, Pre-1.91 Ga deformation and metamorphism in the Palaeoproterozoic Vammala Migmatite Belt, southern Finland, and implications for Svecofennian tectonics: Bulletin of the Geological Society of Finland, v. 76, no. 1–2, p. 93–140.

Salli, I., 1964, The structure and stratigraphy of the Ylivieska-Himanka schist area, Finland: Geological Survey of Finland, v. 211.

Savunen, J., 2015, Hirsikangas orogenic gold deposit and its relation to the metamorphic evolution of the Pohjanmaa schist: University of Turku. (unpublished MSc thesis)

Sayab, M., 2009, Tectonic significance of structural successions preserved within low-strain pods: Implications for thin- to thick-skinned tectonics vs. multiple near-orthogonal folding events in the Palaeo-Mesoproterozoic Mount Isa Inlier (NE Australia): Precambrian Research, v. 175, no. 1–4, p. 169–186, doi: 10.1016/j.precamres.2009.09.007.

Scherrer, N.C., Engi, M., Gnos, E., Jakob, V., and Liechti, A., 2000, Monazite analysis ; from sample preparation to microprobe age dating and REE quantification: Schweiz. Mineral. Petrogr. Mitt., v. 80, p. 93–105.

Shaw, J., and Johnston, S.T., 2012, The carpathian-balkan bends: An oroclinal record of ongoing Arabian-Eurasian collision: Journal of the Virtual Explorer, v. 43, p. 4, doi: 10.3809/jvirtex.2012.00310.

Shaw, J., Johnston, S.T., Gutiérrez-Alonso, G., and Weil, A.B., 2012, Oroclines of the Variscan orogen of Iberia: Paleocurrent analysis and paleogeographic implications: Earth and Planetary Science Letters, v. 329–330, p. 60–70, doi: 10.1016/j.epsl.2012.02.014.

Shaw, J., Johnston, S.T., and Gutiérrez-Alonso, G., 2016, Orocline formation at the core of Pangea: A structural study of the Cantabrian orocline, NW Iberian Massif: Lithosphere,

v. 8, no. 1, p. 97, doi: 10.1130/L461.1.

Skytta, P., Vaisanen, M., and Manttari, I., 2006, Preservation of Palaeoproterozoic early Svecofennian structures in the Orij??rvi area, SW Finland-Evidence for polyphase strain partitioning: Precambrian Research, v. 150, no. 3–4, p. 153–172, doi: 10.1016/j.precamres.2006.07.005.

Skytta, P., and Manttari, I., 2008, Structural setting of late Svecofennian granites and pegmatites in Uusimaa Belt, SW Finland: Age constraints and implications for crustal evolution: Precambrian Research, v. 164, no. 1–2, p. 86–109, doi: 10.1016/j.precamres.2008.04.001.

Smith, H.A., and Barreiro, B., 1990, Monazite U-Pb dating of staurolite grade metamorphism in pelitic schists: Contributions to Mineralogy and Petrology, v. 105, no. 5, p. 602–615, doi: 10.1007/BF00302498.

Torvela, T., Manttari, I., and Hermansson, T., 2008, Timing of deformation phases within the South Finland shear zone, SW Finland: Precambrian Research, v. 160, no. 3–4, p. 277–298, doi: 10.1016/j.precamres.2007.08.002.

Vaisanen, M., and Hölttä, P., 1999, Structural and metamorphic evolution of the Turku migmatite complex, southwestern Finland: Bulletin of the Geological Society of Finland, v. 71, no. 1, p. 177–218.

Vaisanen, M., Manttari, I., and Hölttä, P., 2002, Svecofennian magmatic and metamorphic evolution in southwestern Finland as revealed by U-Pb zircon SIMS geochronology: Precambrian Research, v. 116, no. 1–2, p. 111–127, doi: 10.1016/S0301-9268(02)00019-0.

Van der Voo, R., 2004, Paleomagnetism, Oroclines, and Growth of the Continental Crust: Geological Society of America Today, v. 14, no. 9, p. 4–10, doi: 10.1130/1052-5173(2004)014<4.

Weil, A.B., Gutiérrez-alonso, G., Johnston, S.T., and Pastor-galán, D., 2013, Tectonophysics Kinematic constraints on buckling a lithospheric-scale orocline along the northern margin of Gondwana : A geologic synthesis: Tectonophysics, v. 582, p. 25–49, doi: 10.1016/j.tecto.2012.10.006.

Williams, M. L., Jercinovic, M. J., & Hetherington, C. J., 2007, Microprobe monazite geochronology: understanding geologic processes by integrating composition and chronology. Annu. Rev. Earth Planet. Sci., 35, 137-175.

Williams, I.S., Rutland, R.W.R., and Kousa, J., 2008, A regional 1.92 Ga tectonothermal episode in Ostrobothnia, Finland: Implications for models of Svecofennian accretion: Precambrian Research, v. 165, no. 1–2, p. 15–36, doi: 10.1016/j.precamres.2008.05.004.

Zwart, H.J., 1962, On the determination of polymetamorphic mineral associations, and its

application to the Bosost Area (Central Pyrenees): Geologische Rundschau, v. 52, no. 1, p. 38–65, doi: 10.1007/BF01840064.

Appendix

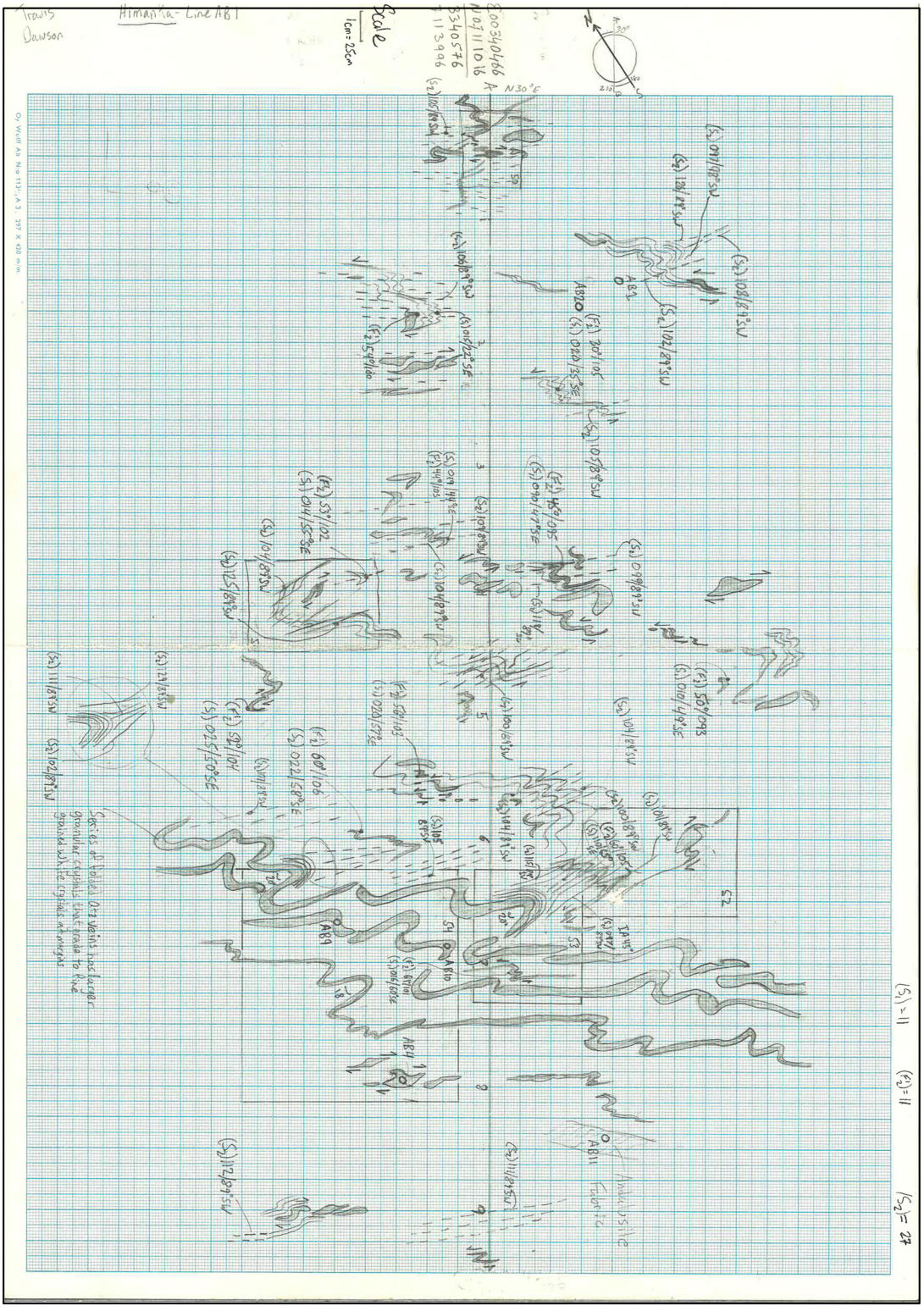

Figure A-1 Field sketch and measurements from transect AB(1)

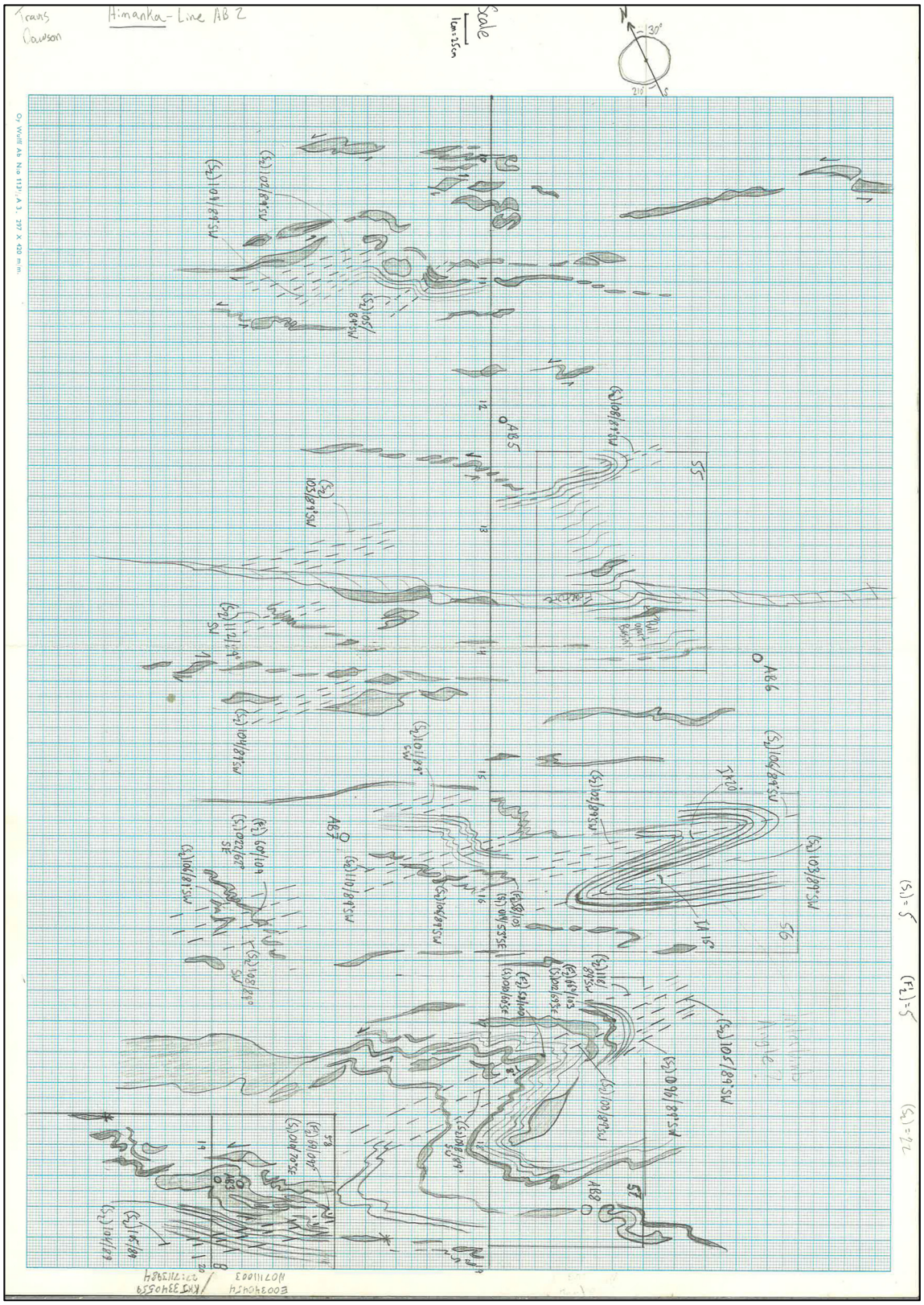

Figure A-2 Field sketch and measurements from transect AB(2)

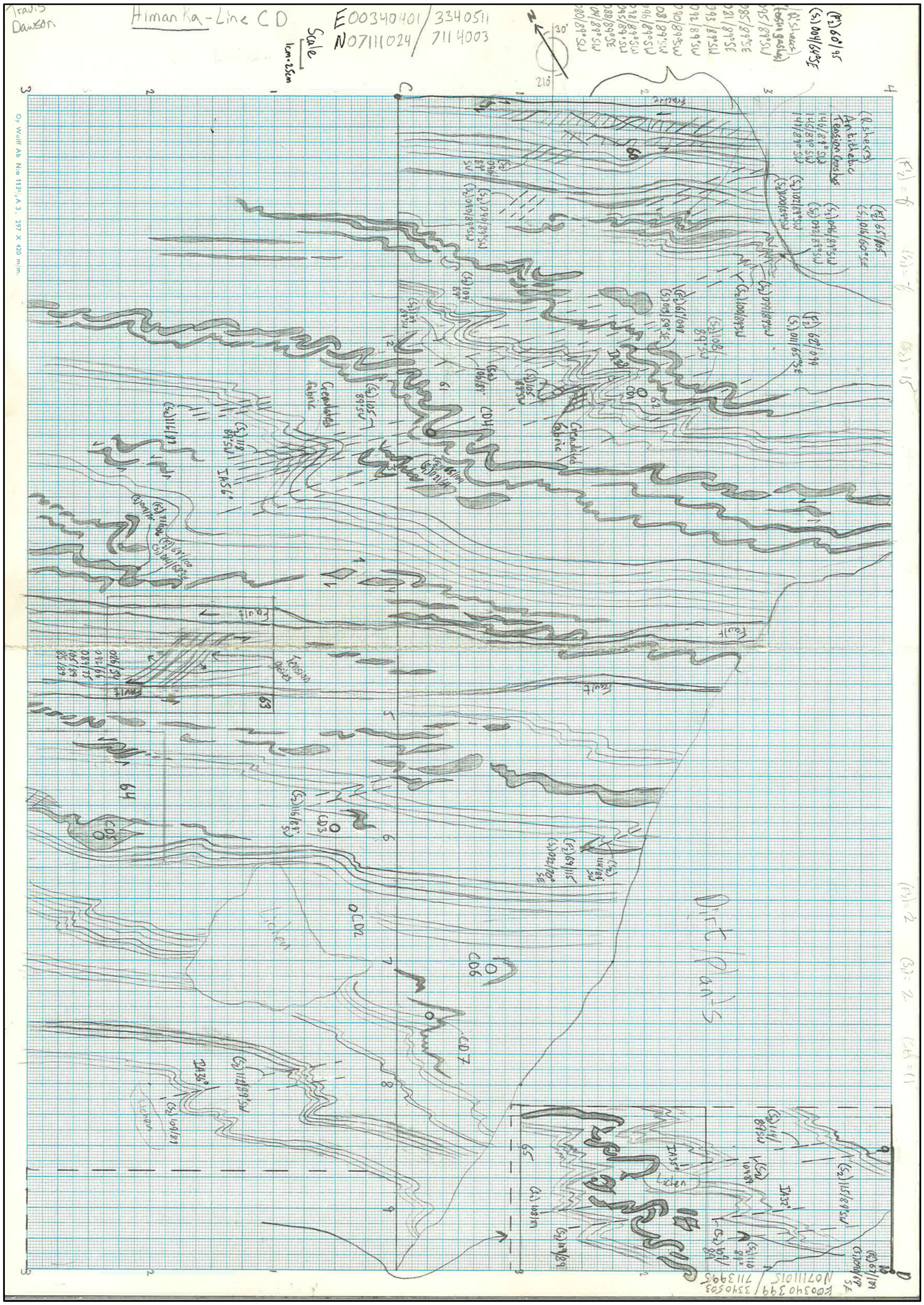

Figure A-3 Field sketch and measurements from transect CD

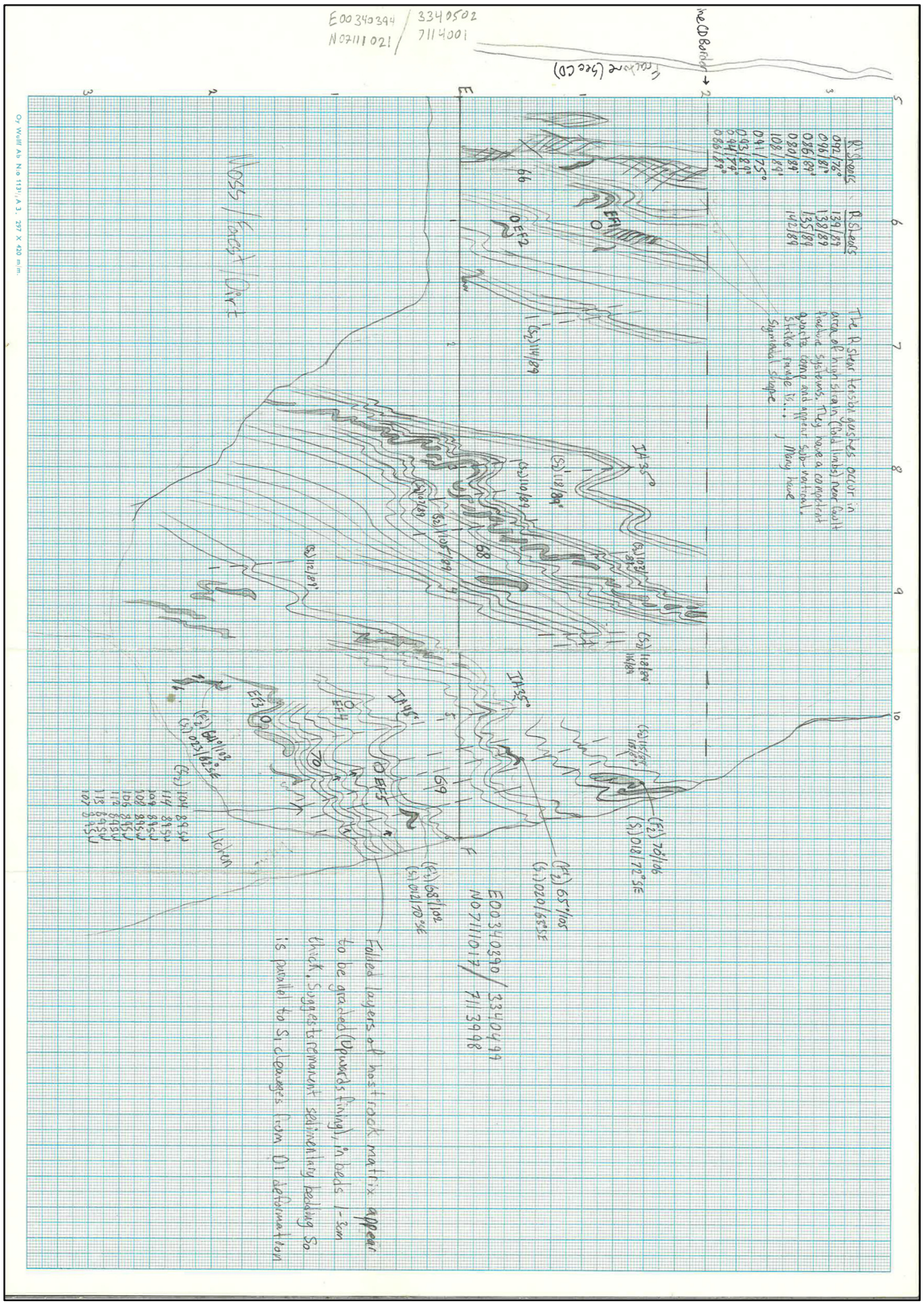

Figure A-4 Field sketch and measurements from transect EF

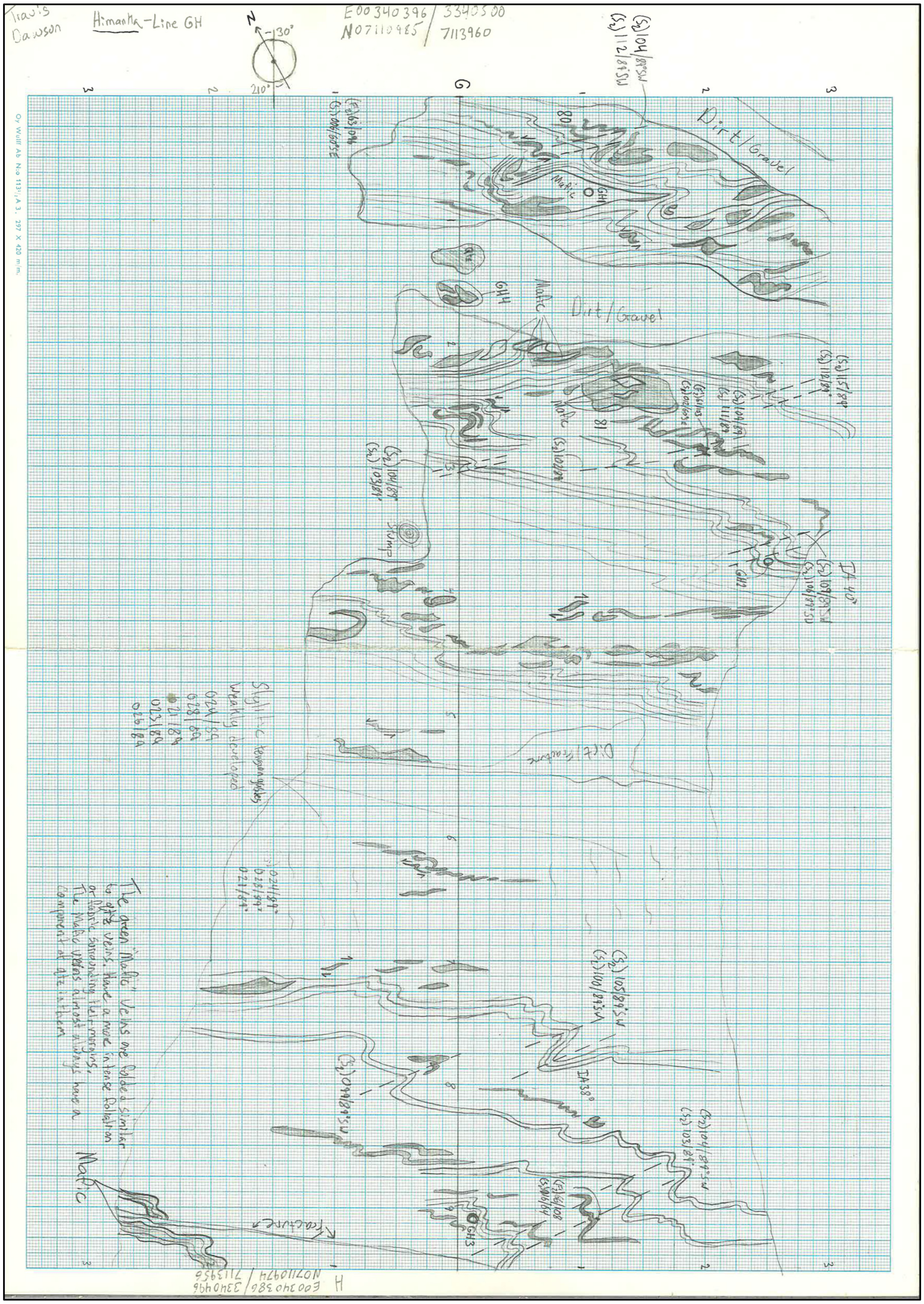

Figure A-5 Field sketch and measurements from transect GH(1)

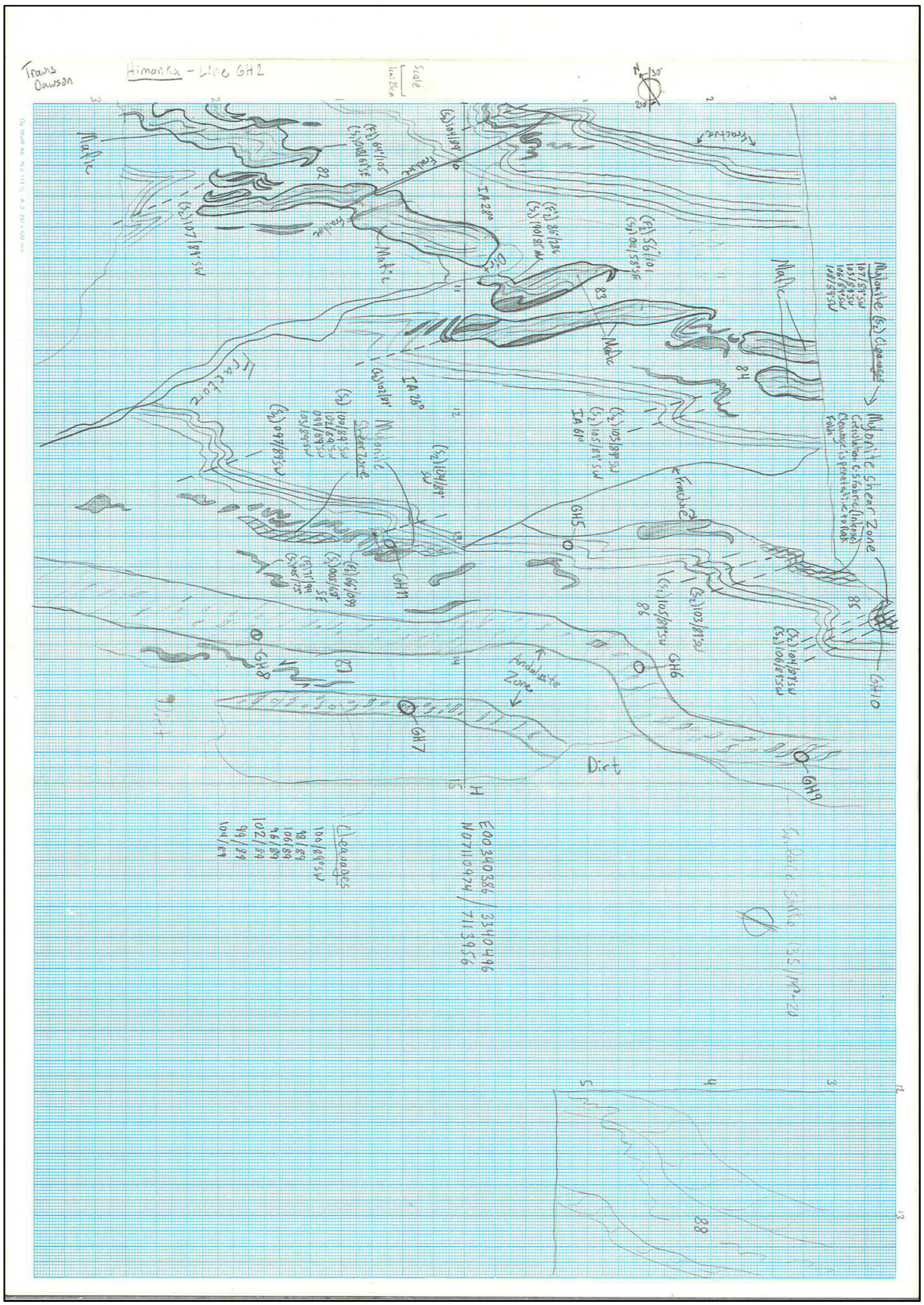

Figure A-6 Field sketch and measurements from transect GH(2)